## **Matter**



## **Article**

# Symbiotic Photosynthetic Oxygenation within 3D-Bioprinted Vascularized Tissues



Three-dimensional-bioprinted unicellular green algae, Chlamydomonas reinhardtii, was used as a sustainable bionic source of  $O_2$  in engineered tissue constructs.  $O_2$  photosynthetically produced by bioprinted algae significantly improved the viability and functionality of the human cells within surrounding matrices while reducing their hypoxic conditions. Fugitive patterns encapsulating the algae were enzymatically dissolved by cellulase digestion to create interconnected microchannels, which were subsequently endothelialized, generating vascularized tissues.

Sushila Maharjan, Jacqueline Alva, Cassandra Cámara, ..., Feng Cheng, Guoliang Ying, Yu Shrike Zhang

yszhang@research.bwh.harvard.edu

#### **HIGHLIGHTS**

Application of bioprinted algae as  $O_2$  generator in tissue (model) engineering

O<sub>2</sub> produced by algae patterns improved functions of surrounding human cells

Endothelialization of channels post-enzymatic digestion of fugitive algae patterns



Maharjan et al., Matter 4, 217–240 January 6, 2021 © 2020 Elsevier Inc. https://doi.org/10.1016/j.matt.2020.10.022



## **Matter**



#### **Article**

## Symbiotic Photosynthetic Oxygenation within 3D-Bioprinted Vascularized Tissues

Sushila Maharjan,<sup>1</sup> Jacqueline Alva,<sup>1</sup> Cassandra Cámara,<sup>1</sup> Andrés G. Rubio,<sup>1</sup> David Hernández,<sup>1</sup> Clément Delavaux,<sup>1</sup> Erandy Correa,<sup>1</sup> Mariana D. Romo,<sup>1</sup> Diana Bonilla,<sup>1</sup> Mille Luis Santiago,<sup>1</sup> Wanlu Li,<sup>1</sup> Feng Cheng,<sup>1</sup> Guoliang Ying,<sup>1</sup> and Yu Shrike Zhang<sup>1,2,\*</sup>

#### **SUMMARY**

In this study, we present the photosynthetic oxygen (O2) supply to mammalian cells within a volumetric extracellular matrix-like construct, whereby a three-dimensional (3D)-bioprinted fugitive pattern encapsulating unicellular green algae, Chlamydomonas reinhardtii, served as a natural photosynthetic O2 generator. The presence of bioprinted C. reinhardtii enhanced the viability and functionality of mammalian cells while reducing the hypoxic conditions within the tissues. We were able to subsequently endothelialize the hollow perfusable microchannels formed after enzymatic removal of the bioprinted C. reinhardtii-laden patterns from the matrices following the initial oxygenation period to obtain biologically relevant vascularized mammalian tissue constructs. The feasibility of co-culture of C. reinhardtii with human cells, the printability and the enzymatic degradability of the fugitive bioink, and the exploration of C. reinhardtii as a natural, eco-friendly, cost-effective, and sustainable source of O<sub>2</sub> would likely promote the development of engineered tissues, tissue models, and food for various applications.

#### **INTRODUCTION**

Millions of people lose their lives on an annual basis due to health issues associated with organ failure. According to the World Health Organization, only about 10% of the global need for organ transplantation is being met as a result of donor organ shortage.<sup>2</sup> Thus, there is an increasing demand for artificial tissue substitutes to replace those that are damaged/diseased to restore tissue and organ functions. Tissue engineering represents a promising approach that aims at in vitro production of functional tissues for clinical transplantation to replace and restore the functions of those that are damaged.<sup>3</sup> Over the past decade, three-dimensional (3D) bioprinting techniques have been explored extensively for fabricating tissue scaffolds for biomedical and tissue-engineering applications. 4 3D bioprinting enables in vitro fabrication of volumetric tissue constructs of predefined architectures and shapes, possibly also with embedded vasculature, by precise positioning of bioinks that are typically composed of hydrogels, cells, and/or bioactive agents. 4-6 Moreover, 3D-bioprinted tissue models, such as those of the liver, heart, skin, muscle, lung, and tumors, have been used to study the pathophysiology of diseases as well as the pharmacokinetics and pharmacodynamics of drugs in vitro.<sup>7-9</sup>

Despite advances in the fabrication of 3D tissues and their models *in vitro*, there are still major limitations such as maintaining high cell viability and functionality

#### **Progress and Potential**

Sufficient and homogeneous distribution of oxygen  $(O_2)$ facilitates cell growth within threedimensional (3D) tissue constructs whereas limited supply of  $O_2$ induces cell death. This work reports the unique adoption of 3D-bioprinted Chlamydomonas reinhardtii as a natural photosynthetic O<sub>2</sub> generator for enhancing functions of engineered tissue constructs in vitro. Interestingly, the cellulase-mediated digestion of the bioprinted C. reinhardtiiladen patterns embedded within mammalian cell-encapsulating GelMA matrices created perfusable and interconnected microchannels. These microchannels, when subsequently endothelialized, made it possible to obtain biologically relevant vascularized tissue constructs. These bioprinted unicellular microalgae represent a bionic and sustainable source of O2, promoting the development of engineered mammalian tissues.







throughout a tissue construct, which is largely determined by the availability of oxygen (O<sub>2</sub>). <sup>10</sup> Sufficient and homogeneous distribution of O<sub>2</sub> facilitates cell growth, <sup>11</sup> and inadequate supply of O<sub>2</sub> has been shown to induce cell death within 3D tissue constructs. 12 In fact, when the thickness of a tissue construct exceeds a few hundred micrometers to a few millimeters, hypoxic condition occurs especially in the central regions, due to the limited diffusion of O<sub>2</sub> into the 3D matrix. <sup>13</sup> Efforts have been made to improve O<sub>2</sub> supply in engineered tissue constructs such as incorporation of O<sub>2</sub>-releasing biomaterials, including sodium percarbonate, <sup>14</sup> magnesium peroxide, 15 calcium peroxide, 16 and hydrogen peroxide, 17 in the form of scaffolds 18 and microspheres, <sup>19</sup> among others. Nevertheless, these O<sub>2</sub>-releasing biomaterials are usually to different levels cytotoxic due to the production of hydrogen peroxide, reactive O2 species, and decomposition of salt by-products affecting the cell viability within the tissue constructs, as well as typically fast and rapidly declining release profiles.<sup>20</sup> Another approach relies on incorporation of vascular channels, with or without relevant cells, within the tissue constructs. 10 3D bioprinting allows rapid fabrication of vascular channels within volumetric tissue constructs using sacrificial (bio)inks, such as Pluronic F127, 13 gelatin, 21 agarose, 22 and hydrocarbons, 23 within the tissue scaffolds, which after removal create perfusable microchannels that can be seeded with vascular cells for angiogenic sprouting and/or implanted in vivo to promote the formation of vascular networks.<sup>24,25</sup>

Very recently, photosynthetic microalgae have been attempted as a source of O<sub>2</sub> in engineered tissue constructs. Bloch et al. described the co-encapsulation of pancreatic islets and unicellular alga, Chlorella sorokiniana, in alginate beads and showed that these microalgae could generate sufficient O<sub>2</sub> for respiration and function of islets under in vitro anoxic environments. They simply mixed islets and C. sorokiniana in sodium alginate and then extruded it through a pipette tip into a calcium chloride solution.<sup>26</sup> Hopfner et al. established the co-culture of Chlamydomonas reinhardtii and murine 3T3 fibroblasts in 3D collagen scaffolds. They seeded C. reinhardtii and fibroblasts on commercially available collagen-based scaffolds and demonstrated that the scaffolds harboring C. reinhardtii produced enough O2, thereby decreasing the hypoxic response under low-O2 culture conditions.<sup>27</sup> Haraguchi et al. reported the fabrication of 3D tissue scaffolds in which Chlorococcum littorale and C2C12 mouse myoblasts or rat cardiac cells were layered one above the other by the cell sheet-engineering approach.<sup>28</sup> This study showed the possibility of an in vitro symbiotic relationship between mammalian cells and algae. Moreover, Lode et al. demonstrated the 3D bioprinting of C. reinhardtii and C. sorokiniana encapsulated in alginate/methylcellulose (3:1) blend by means of extrusion bioprinting and demonstrated the growth rate and viability of the bioprinted microalgae.<sup>29</sup> These authors also fabricated the patterned human SaOS-2 cells and C. reinhardtii co-cultured 3D scaffolds by alternate plotting of hydrogel laden with SaOS-2 and C. reinhardtii. In this pioneering work, the potential of 3D bioprinting for creation of patterned human cell/algae co-culture scaffolds was briefly demonstrated, yet the structures produced were less physiologically relevant, as the fully exposed porous patterns did not seem to take advantage of the oxygenation by the algae.

Here, we present 3D fabrication of perfusable vascularized tissue constructs via bioprinting of photosynthetic *C. reinhardtii* encapsulated in a sacrificial cellulose-based blend bioink with predesigned geometries. Cellulose is the water-insoluble natural polymer of glucose and is the main structural component of plants, algae, and fungi, which provides them with the mechanical strength and maintains the structural integrity. <sup>30,31</sup> Cellulose-based hydrogels are prepared from water-soluble ether derivatives of cellulose, such as methylcellulose, ethyl cellulose, hydroxyethyl cellulose,

<sup>&</sup>lt;sup>1</sup>Division of Engineering in Medicine, Department of Medicine, Brigham and Women's Hospital, Harvard Medical School, Cambridge, MA 02139, USA

<sup>&</sup>lt;sup>2</sup>Lead Contact

<sup>\*</sup>Correspondence: yszhang@research.bwh.harvard.edu https://doi.org/10.1016/j.matt.2020.10.022





hydroxypropyl methylcellulose, and sodium carboxymethylcellulose, through physical or chemical crosslinking. <sup>30,32</sup> Carboxymethyl cellulose sodium salt (NaCMC) can also be used as a rheology-modifier, stabilizer, and thickener in a wide range of formulations. <sup>33</sup>

As a proof-of-principle demonstration, we embedded the bioprinted *C. reinhardtii*-containing sacrificial structures within gelatin methacryloyl (GelMA)-based hydrogel constructs harboring liver-derived cells, and evaluated the availability of O<sub>2</sub> produced by the bioprinted *C. reinhardtii* as well as their ability to support the viability and functions of human liver-derived cells within the tissue constructs. We subsequently investigated the feasibility of forming hollow microchannels following culture and enzymatic removal of the bioprinted *C. reinhardtii* patterns and of seeding endothelial cells in the microchannels to obtain vascularized hepatic tissue-like constructs. Development of such a fugitive bioink that allows initial oxygenation and subsequent vessel formation within a single tissue construct has not been reported, which however is a critical step toward successful engineering of viable and functional tissues.

#### **RESULTS**

#### 3D Bioprinting of the NaCMC-Based Bioink

The bioink was prepared by homogeneously mixing different amounts of NaCMC, poly(vinyl alcohol) (PVA), gelatin, and alginate solutions. NaCMC and gelatin were utilized as the main components, while PVA and alginate as the additives. During bioprinting, a suitable viscosity of the bioink is important to ensure its proper extrusion.<sup>34</sup> Deformation and collapse can easily happen when bioprinting low-viscosity materials; on the other hand, nozzles may be frequently jammed when high-viscosity bioinks are used. We therefore examined the printability of bioink formulations with different concentrations of NaCMC (3%-10% v/v), PVA (0.01%-0.1% v/v), gelatin (2%-10% w/v), and alginate (0.5%-1% w/v), at different pressures (35-60 psi) as well as at different feeding rates (60–100 mm s $^{-1}$ ). The printability studies revealed the optimal bioink formulation as 3% (v/v) NaCMC, 0.03% (v/v) PVA, 4% (v/v) gelatin, and 0.8% (v/v) alginate at 55 psi of pressure and 70 mm s<sup>-1</sup> of feeding rate when a 27-gauge extrusion needle was used (Tables S1 and S2; Figure S1). The appropriate amounts of gelatin and alginate were added to improve the printability of the bioink and to stabilize the shapes of the bioprinted structures. The polymer-polymer interactions for the formation of the hydrogel were mainly due to the intermolecular and/ or intramolecular hydrogen bonding among the functional groups<sup>35</sup> of the different components (Figure 1A). Indeed, the viscosity of the optimized bioink was found to be higher compared with individual components when measured as a function of shear rate (Figure 1B).

The optimized bioink was then applied to fabricate honeycomb-shaped 3D constructs at room temperature under the optimized pressure and feeding rate. The schematic illustration of the bioprinting process is shown in Figure 1C. The honeycomb construct comprised seven hexagonal lobules with each lobule having a circumradius of 1.6 mm, and the length of each side of the hexagon was 1.6 mm. Immediately after bioprinting, the 3D honeycomb constructs were transferred into a 0.3-M calcium chloride (CaCl<sub>2</sub>) bath and incubated for 5 min to physically crosslink the alginate component of the constructs. The fabrication of 3-, 4-, 6-, 10-, and 20-layered honeycomb constructs was achieved under optimized conditions. Figure 1D illustrates the representative photographs of 3-, 4-, 6-, 10-, and 20-layered honeycomb constructs with the respective side views in the top insets. Furthermore, 3D tubular,





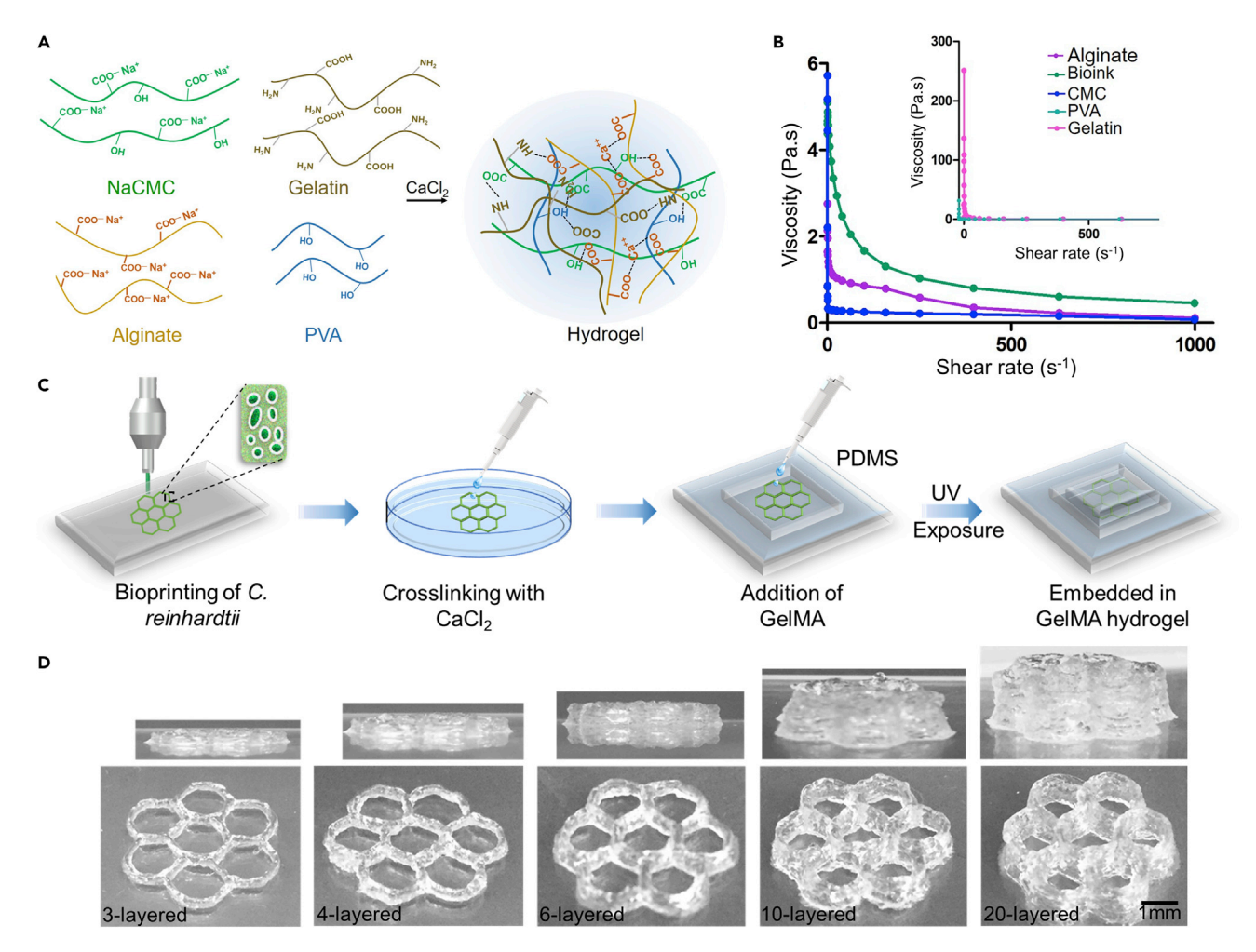


Figure 1. Formulation of the Fugitive Bioink and 3D Bioprinting

- (A) Schematics of the bioink formulation.
- (B) Viscosity characterizations of the optimized bioink and the different components of the bioink.
- (C) Schematic illustration of the 3D-bioprinting process.
- (D) Photographs of side and top views of the 3D-bioprinted honeycomb patterns with different layers.

grid, and crossed-grid constructs were printed to demonstrate the ability to extrude complex patterns with different aspect ratios and structures using the optimized bio-ink (Figure S2). Specifically, the 20-layered tubular pattern was 16 mm in diameter while the 20-layered grid and crossed-grid patterns were 20 mm  $\times$  20 mm (length  $\times$  width) and 36 mm  $\times$  22 mm (length  $\times$  width), respectively.

#### **Enzymatic Digestion of the Bioprinted NaCMC-Based Sacrificial Patterns**

We next demonstrated the unique utility of NaCMC-based hydrogel as a sacrificial structure by cellulase-mediated digestion of NaCMC. Cellulase is an enzyme that hydrolyzes cellulose and some related polysaccharides to produce soluble sugars. Among the water-soluble cellulose ethers, NaCMC is the only polyelectrolyte that is sensitive to pH. Thus, we investigated the digestion of the bioprinted NaCMC-based patterns with cellulase at different concentrations (1–5 mg mL<sup>-1</sup>) using two different buffers (citrate and acetate buffers) and at different pH values (5, 6, and 7). While the cellulase was found to be inactive in acetate buffer at all concentrations and pH values studied, it was less active in citrate buffer at pH 5 and pH 7. The optimal concentration of cellulase for complete digestion of the bioprinted

## **Matter** Article



NaCMC-based patterns was found to be 1 mg mL $^{-1}$  at pH 6 in citrate buffer at both 25°C and 37°C. However, the cellulase digestion of the NaCMC-based patterns took longer ( $\sim$ 6 h) at 25°C compared with that at 37°C ( $\sim$ 2 h). Similarly, we also studied the digestion of the bioprinted NaCMC-based patterns embedded within GelMA to create perfusable microchannels under optimized conditions at both 25°C and 37°C. As expected, the digestion of the NaCMC-patterns within GelMA took comparatively longer when incubated with cellulase (1 mg mL $^{-1}$  in citrate buffer, pH 6) at both 25°C and 37°C, yet both leaving behind the clear open microchannels post digestion (Figure S3). At 25°C, it took approximately 12 h while at 37°C it took about 4 h. We further confirmed the formation of interconnected lumens within GelMA constructs by the perfusion of colored microbeads, as shown in Video S1.

#### 3D Bioprinting of C. reinhardtii-Laden Patterns

The excellent biocompatibility, bioadhesive properties, and cellulase-mediated degradation<sup>38</sup> of NaCMC have prompted the use of NaCMC-based hydrogel as the fugitive matrix for the bioprinting of photosynthetic algae, C. reinhardtii. Different concentrations of freshly pelleted C. reinhardtii (1.0–10  $\times$  10<sup>6</sup> cells mL<sup>-1</sup>) were mixed with the bioink and bioprinted following the same procedure as those without the algae. The density of 5  $\times$  10<sup>6</sup> cells mL<sup>-1</sup> of C. reinhardtii was found to be optimum for bioprinting. The addition of the C. reinhardtii did not noticeably affect the printability of the bioink as well as the crosslinking, resulting in stable constructs with predefined geometries. As such, 4-, 6-, 10-, and 20-layered C. reinhardtii-laden 3D honeycomb structures were fabricated using  $5 \times 10^6$  C. reinhardtii cells mL<sup>-1</sup>. Due to the transparency of the bioink, the homogeneous distribution of green C. reinhardtii was clearly visible within the bioprinted patterns of various heights and thicknesses (Figure 2A). Similarly, 20-layered C. reinhardtii-laden tubular, grid, and crossed-grid constructs were printed demonstrating the faithful extrusion of different patterns of C. reinhardtii-laden structures (Figure 2B). The 20-layered C. reinhardtii-laden tubular pattern was 16 mm in diameter while the 20-layered C. reinhardtii-laden grid and C. reinhardtii-laden crossed-grid patterns were 20 mm x 20 mm (length × width) and 36 mm × 22 mm (length × width), respectively. Immediately after bioprinting, the C. reinhardtii-laden patterns were placed in 0.3-M CaCl<sub>2</sub> bath for 5 min and then incubated in Tris-acetate-phosphate (TAP) medium at 25°C under continuous light illumination (light intensity 2,800 lux). While the C. reinhardtii-laden structures were light green at day 1, they appeared dark green after 7 days of cultivation (Figure 2C). The growth of C. reinhardtii within bioprinted pattern was observed both macroscopically and microscopically (Figure 2C).

The viability and growth of *C. reinhardtii* within the bioprinted patterns were further confirmed by both live and dead assays using Sytox-orange dye and measuring optical density (OD) values at 750 nm. The bioprinted *C. reinhardtii* was incubated in the TAP medium at 25°C under continuous light illumination (2,800 lux), and live/dead assay was performed at day 14. The Sytox-orange dye could penetrate damaged cell membranes and therefore stain dead cells in orange, while viable cells were visualized utilizing the red autofluorescence of chlorophyll (Figure 2D). The viability of the bioprinted *C. reinhardtii* was about 90% at day 1, which gradually increased with time and reached roughly 98% at day 14 (Figure 2E). Similarly, macroscopic, microscopic, and OD<sub>750</sub> measurements using a microplate reader for the bioprinted *C. reinhardtii* within 4-layered (Figures S4A and S4B), 6-layered (Figures S4C and S4D), and 10-layered (Figures S4E and S4F) honeycomb structures also revealed a gradual increase of the *C. reinhardtii* density over the culture period of 14 days. The cell density of *C. reinhardtii* was proportional to the number of layers

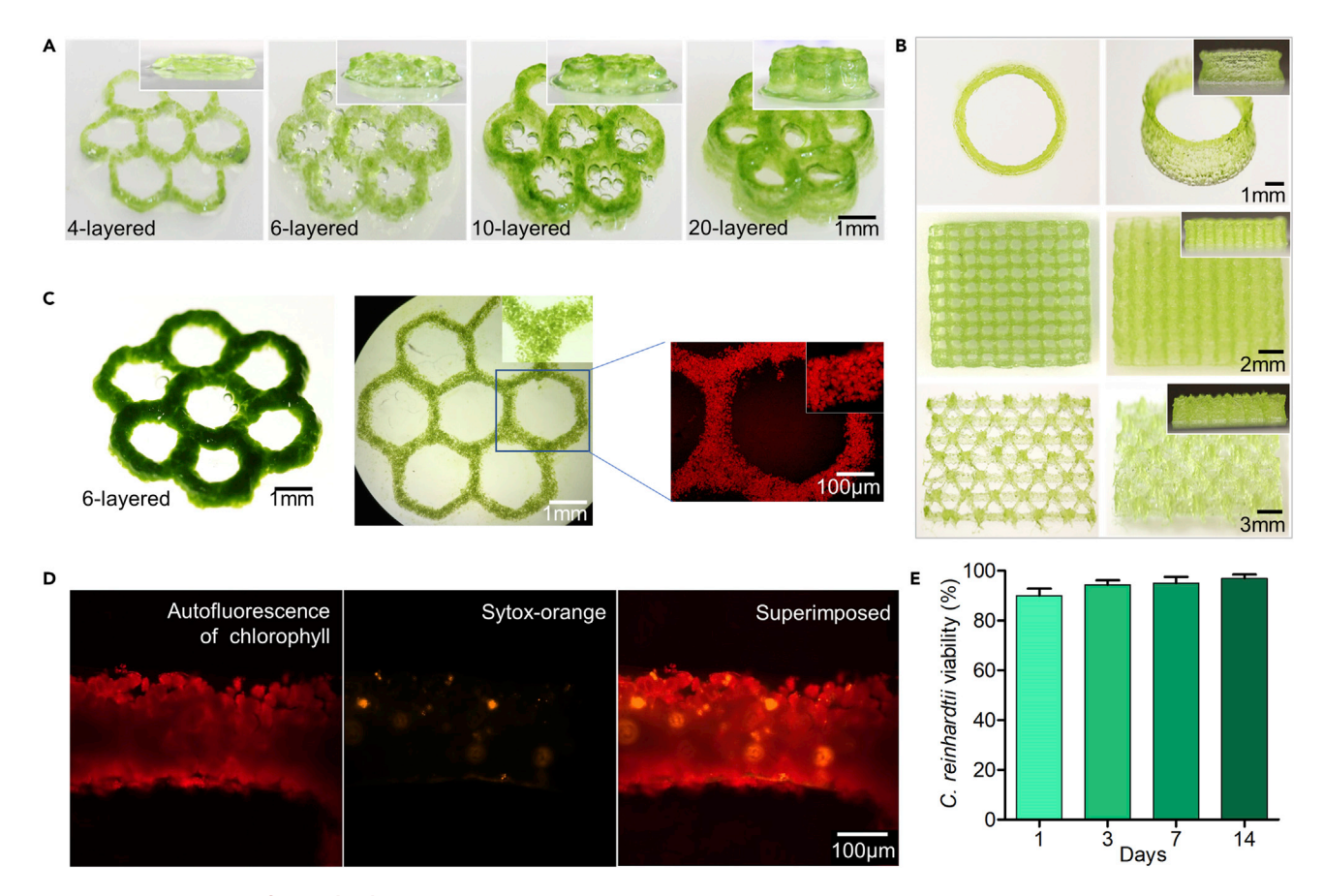


Figure 2. 3D Bioprinting of C. reinhardtii

- (A) Photographs showing bioprinted C. reinhardtii-laden honeycomb patterns with different layers at day 3.
- (B) Photographs of bioprinted C. reinhardtii-laden tubular, grid, and cross-grid patterns with different sizes.
- (C) Optical and fluorescence micrographs of bioprinted C. reinhardtii-laden honeycomb patterns.
- (D) Viability of C. reinhardtii at different days determined by live/dead assay using Sytox-orange.
- (E) Viability of the bioprinted C. reinhardtii within 4-layered honeycomb patterns at different days, as represented by  $OD_{750}$ . Results are presented as means  $\pm$  standard deviations.

in the honeycomb structures demonstrating uniform growth of the algae throughout the bioprinted patterns.

Since we aimed to use the bioprinted C. reinhardtii as the source of  $O_2$  for mammalian cells in tissue constructs, we next studied the growth of C. reinhardtii within 3D-bioprinted patterns at 37°C and compared it with that at 25°C, both under continuous light-illumination conditions (2,800 lux). C. reinhardtii within the bioprinted structures exhibited similar growth behaviors at 37°C as observed at 25°C, over the 14 days of culture period when cultured in TAP medium (Figure S5). A gradual increase of the C. reinhardtii density was observed over the culture period of 14 days at 37°C within 4-layered (Figures S5A and S5B), 6-layered (Figures S5C and S5D), and 10-layered (Figures S5E and S5F) honeycomb structures. We further investigated the growth of C. reinhardtii in commonly used mammalian cell-culture medium, Dulbecco's modified Eagle's medium (DMEM) supplemented with 10% fetal bovine serum (FBS) and 1% penicillin/streptomycin (P/S), for 7 days and compared it with that in DMEM/TAP medium (1:1) and TAP medium, at both 25°C and 37°C under mammalian cell-culture conditions and continuous light illumination (2,800 lux). At both 25°C and 37°C, C. reinhardtii showed reduced growth in DMEM

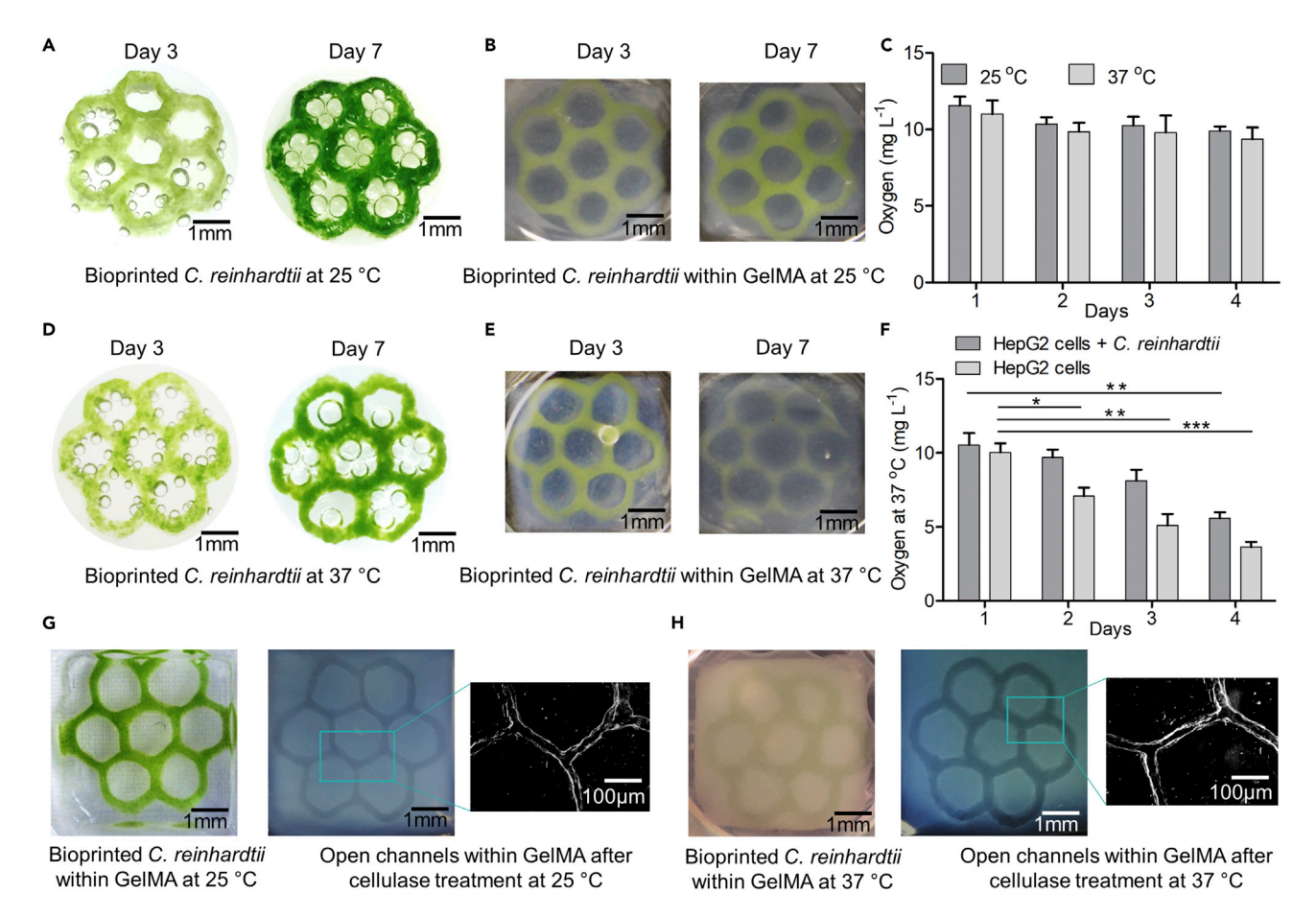


Figure 3. Growth of Bioprinted C. reinhardtii and Measurements of Dissolved O<sub>2</sub> Levels in Medium

- (A) Photographs showing the bioprinted C. reinhardtii grown in TAP medium at 25°C.
- (B) Photographs showing the bioprinted C. reinhardtii within a GelMA scaffold grown in TAP medium at 25 °C.
- (C) Levels of dissolved  $O_2$  released by bioprinted C. reinhardtii in TAP medium at 25°C and 37°C. Results are presented as means  $\pm$  standard deviations.
- (D) Photographs showing the bioprinted C. reinhardtii grown in DMEM/TAP medium (1:1) at  $37^{\circ}C$ .
- (E) Photographs showing the bioprinted C. reinhardtii within a GelMA scaffold grown in DMEM/TAP medium (1:1) at 37°C.
- (F) Levels of dissolved  $O_2$  in DMEM/TAP medium (1:1) at 37°C in the presence or absence of bioprinted *C. reinhardtii* embedded within GelMA/HepG2 matrices. Results are presented as means  $\pm$  standard deviations. \*p  $\leq$  0.05, \*\*p  $\leq$  0.01, \*\*\*p  $\leq$  0.001.
- (G) Photographs showing the bioprinted C. reinhardtii pattern within a GelMA matrix at day 7 and the formation of open microchannels within the matrix after digestion of the C. reinhardtii pattern with 1 mg mL $^{-1}$  of cellulase in citrate buffer (pH 6) at 25°C for 12 h, followed by microscopic image showing the open microchannel.
- (H) Photographs showing the bioprinted C. reinhardtii pattern within a GelMA matrix at day 7 and the formation of open microchannels within the matrix after digestion of the C. reinhardtii pattern with 1 mg mL $^{-1}$  of cellulase in citrate buffer (pH 6) at 37°C for 4 h, followed by microscopic image showing the open microchannel.

when compared with DMEM/TAP medium and TAP media (Figure S6). When bioprinted *C. reinhardtii* honeycomb patterns were cultured in DMEM/TAP medium (1:1) at 37°C under mammalian cell-culture conditions, *C. reinhardtii* within the bioprinted structures exhibited similar growth over the period of 4 days of culture as that observed at 25°C, but the growth decreased gradually after day 4 due to the presence of P/S in the DMEM (Figures 3A and 3D). Similar growth of *C. reinhardtii* was observed when the *C. reinhardtii*-laden patterns were embedded in GelMA matrices at both 25°C and 37°C (Figures 3B and 3E). The effect of P/S on the growth of *C. reinhardtii* was confirmed by observing the growth of bioprinted *C. reinhardtii* patterns over the period of 14 days in the presence or absence of 1% P/S in TAP medium (Figure S7) at both 25°C and 37°C. The growth of *C. reinhardtii* within





bioprinted patterns declined gradually over time, approaching negligible growth at day 14. We then assessed the co-culture of mammalian cells such as HepG2 cells and C2C12 cells with *C. reinhardtii* in DMEM/TAP medium (1:1) for 4 days at 37°C and found that these mammalian cells could grow well together with *C. reinhardtii* when cultured under normal mammalian cell-culture conditions (Figure S8). Thus, DMEM/TAP medium (1:1) was chosen as co-culture medium for further cell experiments. We also studied the effect of low light intensity (0 lux) and high light intensity (11,000 lux) on the growth of *C. reinhardtii* at 25°C and 37°C. *C. reinhardtii* did not grow at all under both low and high light intensities studied, indicating that absence of light or presence of too much light were not favorable for the growth of *C. reinhardtii* at both temperatures.

As the bioprinted C. reinhardtii was intended to serve as the source of  $O_2$  to boost the growth of mammalian cells encapsulated in the GelMA hydrogel, we also assessed the effect of UV exposure on C. reinhardtii by measuring  $OD_{750}$  and  $OD_{665}$  using a microplate reader for viability and chlorophyll content, respectively. Bioprinted C. reinhardtii patterns were exposed to different UV levels (0, 18, 45, and 72 mW cm $^{-2}$ ) for 40 s and incubated for 7 days at 25°C and 37°C. At day 7, the growth of C. reinhardtii within bioprinted patterns was measured at  $OD_{750}$ , whereas the chlorophyll was further extracted from the C. reinhardtii using 95% ethanol and read at  $OD_{665}$ . The  $OD_{750}$  and  $OD_{665}$  evaluations revealed that the range of UV tested had no noticeable adverse effect on the growth and the chlorophyll content of the C. reinhardtii within bioprinted structures at both 25°C and 37°C (Figure S9).

#### O<sub>2</sub> Release by Bioprinted C. reinhardtii

The photosynthetic activity of the bioprinted *C. reinhardtii* was demonstrated by measuring the  $O_2$  released in the medium by photoautotrophic growth of *C. reinhardtii* within the constructs. Dissolved  $O_2$  present in the TAP medium was first removed by flushing with a nitrogen gas for 20 min, followed by incubation with the bioprinted *C. reinhardtii* patterns at 25°C and/or 37°C. The  $O_2$  released by bioprinted *C. reinhardtii* was measured by changes of dissolved  $O_2$  concentration in the medium. Under continuous light illumination (2,800 lux) at 25°C, the  $O_2$  concentration in the medium was found to be 11.5 mg L<sup>-1</sup> within the first 24 h. The concentration of dissolved  $O_2$  remained almost at a similar level (~10.5 mg L<sup>-1</sup>) over the period of 4 days at 25°C (Figure 3C). A similar level of dissolved  $O_2$ , 10.9 mg L<sup>-1</sup>, was found over the culture period of 4 days when the bioprinted *C. reinhardtii* patterns were incubated at 37°C under continuous light illumination (2,800 lux), indicating the significant photosynthetic activity of the bioprinted *C. reinhardtii* at 37°C (Figure 3C).

It is well-known that light is an important factor in a photosynthetic process. To gain more insight into how light affects the  $O_2$ -releasing ability of the bioprinted C. reinhardtii, we further investigated the growth and the subsequent release of  $O_2$  by the bioprinted C. reinhardtii patterns under limited light supplies at both  $25^{\circ}C$  and  $37^{\circ}C$ . To study the effect of the attenuation of light, we placed the cylindrical C. reinhardtii-laden matrices of approximately 6-cm height and 2-cm diameter in black bioreactors such that C. reinhardtii scaffolds received light only from the top while light exposure to all other directions was prevented. The C. reinhardtii-laden constructs were incubated in TAP medium for 7 days, and the growth of the algae and their  $O_2$  production were assessed. The C. reinhardtii-laden constructs that were incubated under normal culture conditions whereby the whole constructs were exposed to normal light source (light intensity 2,800 lux) were considered as controls. At both  $25^{\circ}C$  and  $37^{\circ}C$ , the C. reinhardtii showed similar behaviors of reduced growth

## **Matter** Article



corresponding to the attenuation of light with depth. While in the control group C. reinhardtii showed uniform growth throughout the cylindrical constructs at both 25°C (Figure S10A) and 37°C (Figure S10C), the growth of C. reinhardtii was observed only within the top regions of the cylindrical matrices placed in dark bioreactors. At both 25°C and 37°C, the growth of C. reinhardtii gradually decreased with depth, and no growth was observed toward the bottom of the constructs placed inside the black bioreactors. As expected, the  $O_2$  production by C. reinhardtii was drastically decreased when the light source was blocked at both 25°C (Figure S10B) and 37°C (Figure S10D).

Likewise, to evaluate the O<sub>2</sub>-production behaviors of bioprinted C. reinhardtii under precisely modulated supplies of light source, C. reinhardtii-laden constructs were subjected to light (2,800 lux)/dark cycles at 1-h intervals at both 25°C and 37°C. When subjected to the 1-h/1-h light/dark cycles at 25°C, the level of dissolved O<sub>2</sub> in medium was found to increase gradually from 5.7 mg  $L^{-1}$  at 1 h to 6.9 mg  $L^{-1}$ over the culture period of 13 h. After 13 h of culture, the level of dissolved O<sub>2</sub> decreased slightly and remained at  $5.9 \text{ mg L}^{-1}$  until the culture period of 20 h. Thereafter, the  $O_2$  level decreased rapidly over time and reached 1.2 mg  $L^{-1}$  at 40 h (Figure \$10E). The bioprinted C. reinhardtii followed a similar trend of O2 release under 1-h/1-h light (2,800 lux)/dark cycles at 37°C (Figure S10F). The level of dissolved O<sub>2</sub> in medium was found to be  $5.5 \text{ mg L}^{-1}$  within 1 h and increased gradually up to 7.1 mg  $L^{-1}$  at 11 h. After 11 h of culture, the level of dissolved  $O_2$  decreased slightly and remained at 6.3 mg  $L^{-1}$  until 17 h. Thereafter, the  $O_2$  level decreased rapidly over time and reached 1.0 mg L<sup>-1</sup> at 40 h. These results suggested consistency of growth of bioprinted C. reinhardtii under 1-h/1hh light/dark cycles at both 25°C and 37°C. The growth of C. reinhardtii decreased drastically after 20 h when subjected to the 1-h/1-h light/dark cycles under both temperature conditions.

We next measured the dissolved  $O_2$  in medium in the presence of bioprinted C. reinhardtii-laden patterns embedded within HepG2 cell-encapsulated GelMA matrices at  $37^{\circ}$ C (Figure 3F) and compared it with that for the control samples wherein the 3D-bioprinted honeycomb patterns without C. reinhardtii were embedded within HepG2 cell-encapsulated GelMA matrices. The dissolved  $O_2$  levels in medium were found to be similar within 24 h in the presence ( $10.5 \text{ mg L}^{-1}$ ) and absence ( $10.0 \text{ mg L}^{-1}$ ) of C. reinhardtii-laden patterns. Interestingly, while the  $O_2$  level was maintained at  $9.6 \text{ mg L}^{-1}$  in the presence of the C. reinhardtii-laden patterns within the next 24 h, the  $O_2$  level decreased rapidly to  $7.0 \text{ mg L}^{-1}$  in the absence of C. reinhardtii-laden patterns, the dissolved  $O_2$  was found to decrease slowly and reached up to  $5.5 \text{ mg L}^{-1}$ , whereas in the absence of C. reinhardtii, the dissolved  $O_2$  decreased rapidly to  $3.6 \text{ mg L}^{-1}$ , over the period of 4 days of culture at  $37^{\circ}C$ . These results demonstrated the photosynthetic activity of the bioprinted C. reinhardtii and consumption of  $O_2$  by HepG2 cells embedded within GelMA matrices.

#### **Fabrication of Vascularized Hepatic Tissue-like Constructs**

Our aim was to utilize the bioprinted C. reinhardtii as the source of  $O_2$  to boost the initial growth of mammalian cells within the *in vitro* tissue constructs and to eventually create the vasculature within the tissues by removing the C. reinhardtii-laden patterns from tissue constructs.

We first examined the digestion of *C. reinhardtii*, after 3 or 4 days of growth in TAP medium in the presence of 1 mg mL<sup>-1</sup> of cellulase at pH 6. It was found that almost all *C. reinhardtii* cells died or became inactivated within 2 h of cellulase treatment at





25°C, as observed by the reduced autofluorescence of chlorophyll as well as ruptured cell walls (Figure S11). We further studied the digestion of the bioprinted C. reinhardtii-laden patterns embedded within GelMA matrices by treatment with 1 mg mL<sup>-1</sup> of cellulase (pH 6) at both 25°C and 37°C. In the control group, the bioprinted honeycomb patterns without C. reinhardtii were embedded within GelMA matrices. The bioprinted C. reinhardtii honeycomb patterns or control patterns embedded within GelMA matrices were cultured in TAP medium at 25°C or 37°C for 4 days. At day 4, the constructs were treated with cellulase (1 mg mL<sup>-1</sup> in citrate buffer at pH 6) to dissolve the embedded C. reinhardtii patterns or control patterns. While the bioprinted C. reinhardtii or control patterns embedded in GelMA matrices were digested completely within  $\sim$ 12 h at 25°C (Figure 3G), it took only  $\sim$ 4 h at 37°C, leaving behind the open channels in the GelMA matrices (Figure 3H). The bioprinted C. reinhardtii patterns embedded within GelMA matrices could be visualized under fluorescence microscopy due to the presence of autofluorescence of chlorophyll. After the enzymatic digestion, the complete removal of the bioprinted C. reinhardtii within HepG2/GelMA matrices was confirmed by observation under the fluorescence microscope, whereby autofluorescence of chlorophyll of C. reinhardtii was no longer discerned. The presence of interconnected lumens was further confirmed by the perfusion of the medium through the microchannels.

We next embedded C. reinhardtii-laden patterns within HepG2-cell-encapsulated GelMA matrices and allowed them to co-culture at 37°C for up to 3 days. While C. reinhardtii-laden patterns embedded within HepG2/GelMA matrices could be visualized under fluorescence microscopy due to the presence of autofluorescence of chlorophyll, the HepG2 cells were stained with CellTracker Blue CMF2HC dye to aid observation (Figure 4A). Based on the above results on the growth of the C. reinhardtii and the  $O_2$  release, the samples were treated with cellulase (1 mg mL<sup>-1</sup> in citrate buffer at pH 6) at day 4 to dissolve the embedded C. reinhardtii-laden patterns. HepG2/GelMA constructs having bioprinted honeycomb patterns without C. reinhardtii embedded served as the control group. The bioprinted C. reinhardtii honeycomb patterns or control patterns embedded within HepG2-cell-encapsulated GelMA matrices were allowed to co-culture in DMEM/TAP medium at 37°C for 4 days. At day 4, the scaffolds were treated with cellulase (1 mg  $mL^{-1}$  in citrate buffer at pH 6) to dissolve the embedded C. reinhardtii patterns or control patterns. As expected, the C. reinhardtii-laden patterns or control honeycomb patterns embedded in HepG2/GelMA matrices were successfully dissolved within 4 h of cellulase treatment at 37°C, leaving behind the open microchannels.

After ensuring successful removal of the bioprinted fugitive C. reinhardtii-laden patterns or control patterns, the HepG2/GelMA scaffolds with open microchannels were further incubated in DMEM at 37°C and 5%  $CO_2$  for further functional studies of the HepG2 cells within the GelMA matrices. Viability and proliferation of HepG2 cells within GelMA matrices were evaluated at day 3 and day 7 after the removal of C. reinhardtii-laden patterns or control patterns by live/dead assay (Figure 4B) and 3-(4,5-dimethylthiazol-2-yl)-5-(3-carboxymethoxyphenyl)-2-(4-sulfophenyl)-2H-tetrazolium (MTS) assay (Figure 4C), respectively. The viability of HepG2 cells was higher when incubated with the bioprinted C. reinhardtii patterns as compared with the control. We also studied the expression of hypoxia-inducible factor  $1\alpha$  (HIF- $1\alpha$ ) by HepG2 cells within the GelMA matrices at day 7 after the removal of C. reinhardtii-laden patterns or control patterns to evaluate whether the  $O_2$  released by C. reinhardtii-laden patterns in the early stages of co-culture was sufficient for the survival and proliferation of the HepG2 cells within the GelMA matrices. Compared with the control group, the expression of HIF- $1\alpha$  by HepG2 cells was significantly lower

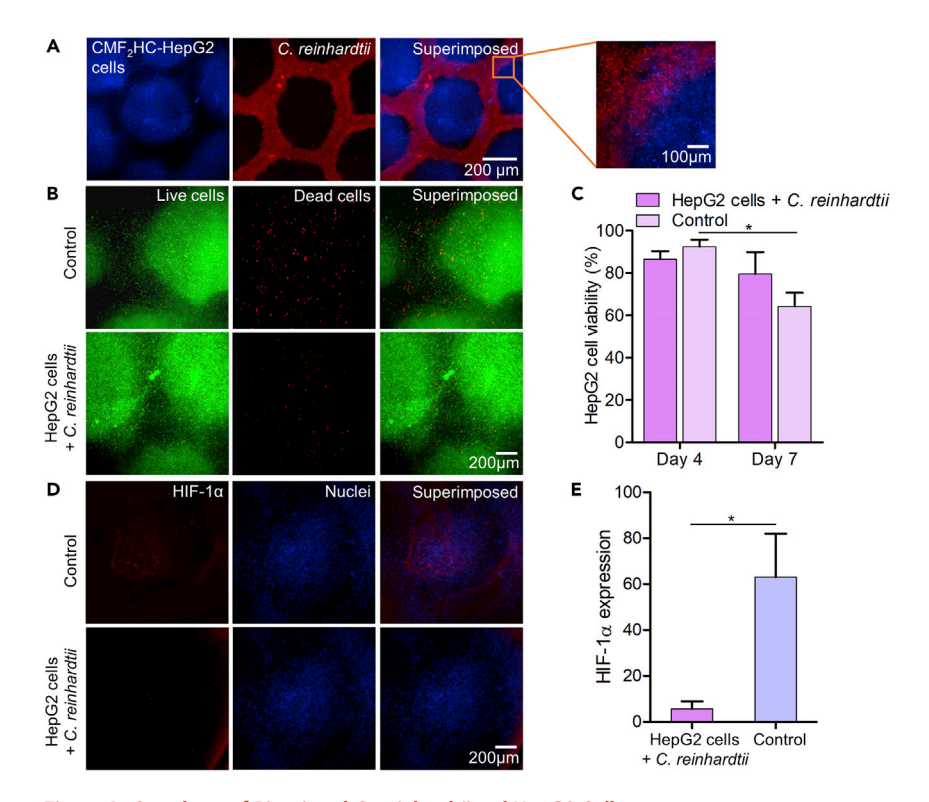


Figure 4. Co-culture of Bioprinted C. reinhardtii and HepG2 Cells

- (A) Fluorescence micrographs showing CellTracker  $CMF_2HC$ -labeled HepG2 cells (blue) in a GelMA construct and the embedded, bioprinted pattern of *C. reinhardtii* (red).
- (B) Fluorescence micrographs showing live (green)/dead (red)-stained HepG2 cells in GelMA constructs at day 4, in the absence (control) or presence of *C. reinhardtii*.
- (C) Viability of HepG2 cells in the absence (control) or presence of *C. reinhardtii*, at day 4 and day 7. Results are presented as means  $\pm$  standard deviations. \*p  $\leq$  0.05.
- (D) Fluorescence micrographs showing the immunostaining of HIF-1 $\alpha$  expression by HepG2 cells in the absence (control) or presence of *C. reinhardtii* at day 7. Nuclei were counterstained with DAPI (blue)
- (E) Quantification of HIF-1 $\alpha$  expression by HepG2 cells in the absence (control) or presence of *C. reinhardtii* at day 7. Results are presented as means  $\pm$  standard deviations. \*p  $\leq$  0.05.

within the GelMA matrices that received  $O_2$  released by C. reinhardtii during the initial 4 days of co-culture (Figures 4D and 4E). Thus, the use of the biosynthetic source of  $O_2$  within the GelMA constructs during the early stages of culture improved the viability/density of the HepG2 cells in the GelMA matrices.

Furthermore, the morphology of the HepG2 cells within the GelMA matrices was evaluated by staining with F-actin, a major component of the cytoskeleton, at day 7 after removal of *C. reinhardtii*-laden patterns or control patterns (Figure 5A). The cells were counterstained with 4′,6-diamidino-2-phenylindole (DAPI) for nuclei. The functionality of HepG2 cells within the GelMA matrices was further confirmed by immunostaining for CYP3A4 and CYP1A2. CYP3A4 and CYP1A2 are the major CYP proteins expressed in liver and are important for the metabolism of drugs.<sup>39</sup> Fluorescence images of the immunostained HepG2 cells within the GelMA matrices exhibited strong expressions of both CYP3A4 (Figure 5B) and CYP1A2 (Figure 5C) compared with the controls. Thus, the expressions of these structural and functional markers by HepG2 cells within the GelMA matrices were observed to be improved when incubated with the bioprinted *C. reinhardtii* patterns during the early stages of culture compared with those in controls.





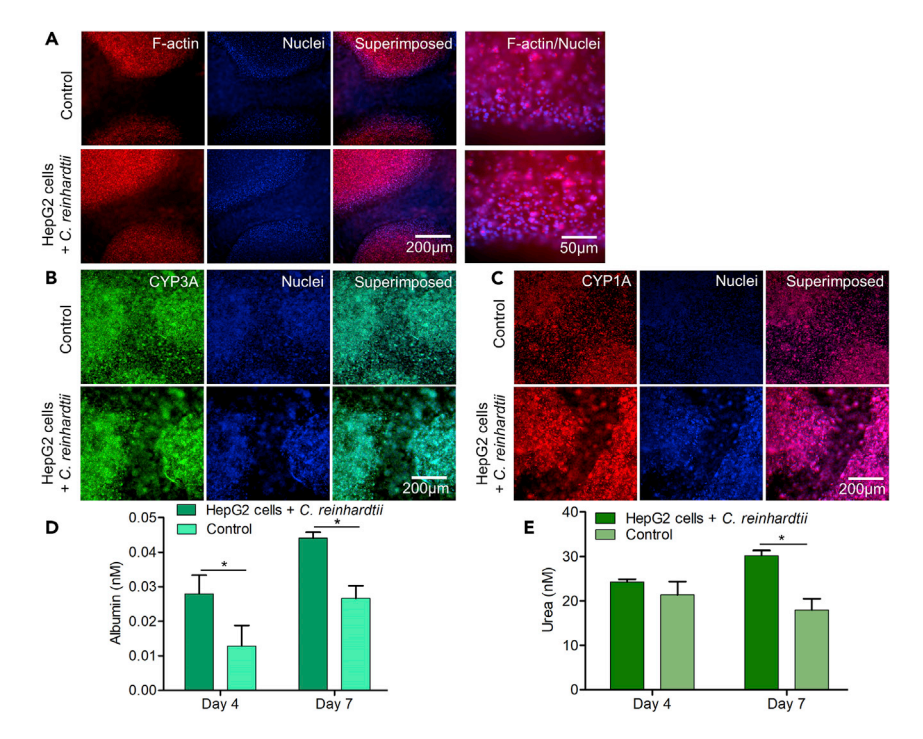


Figure 5. Functional Studies of HepG2 Cells

- (A) Fluorescence micrographs showing the expression of F-actin (red) by HepG2 cells within a GelMA construct at day 7 in the absence (control) and presence of *C. reinhardtii*. Nuclei were counterstained with DAPI (blue).
- (B) Fluorescence micrographs showing the expression of CYP3A (green) by HepG2 cells within a GelMA construct at day 7 in the absence (control) and presence of *C. reinhardtii*. Nuclei were counterstained with DAPI (blue).
- (C) Fluorescence micrographs showing the expression of CYP1A (red) by HepG2 cells within a GelMA construct at day 7 in the absence (control) and presence of *C. reinhardtii*. Nuclei were counterstained with DAPI (blue).
- (D) Albumin secretion by HepG2 cells in GelMA constructs as determined by ELISA. Results are presented as means  $\pm$  standard deviations. \*p  $\leq$  0.05.
- (E) Urea production by HepG2 cells in GelMA constructs as determined by ELISA. Results are presented as means  $\pm$  standard deviations. In all these functional studies, the bioprinted C. reinhardtii-laden patterns within the HepG2/GelMA constructs were dissolved at day 4 by cellulase digestion. \*p  $\leq$  0.05.

In addition, we measured the albumin and urea production by HepG2 cells within the GelMA matrices by ELISA. Both the albumin (Figure 5D) and urea (Figure 5E) secretions were shown to be higher when HepG2 cells were co-cultured with the bioprinted *C. reinhardtii*-laden patterns during the early stages in comparison with the respective controls. Thus, enzymatic digestion of bioprinted *C. reinhardtii* or control patterns within HepG2/GelMA matrices with 1 mg mL $^{-1}$  cellulase in citrate buffer (pH 6) for 4 h did not have any negative influence on the HepG2 cells within the GelMA matrices, where the cells maintained higher levels of viability as well as liver-specific functions, including albumin production and urea synthesis, when compared with the controls. Prior to the enzymatic digestion of *C. reinhardtii*-laden patterns within HepG2/GelMA matrices, the effect of citrate buffer (pH 6) was assessed on the HepG2 cells and C2C12 cells using the same amount of buffer as used for the enzymatic digestion. These cells were cultured in 2 mL of DMEM complete medium containing 400  $\mu$ L of citrate buffer (pH 6) and incubated at 37°C and 5% CO2 in an incubator for 2 days. Any adverse effect of the buffer (pH 6) was not observed on the growth and viability of the cell types tested.

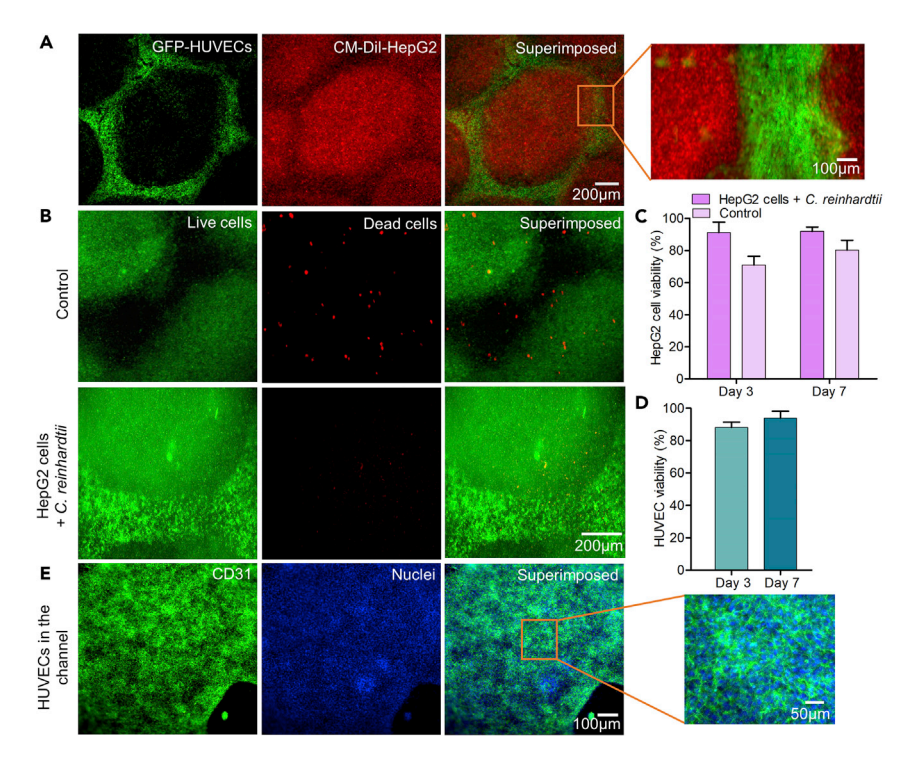


Figure 6. Vascularization of Microchannels

(A) Fluorescence micrographs showing GFP-HUVECs (green) seeded in the channels surrounded by CM-Dil-stained HepG2 cells (red) in a GelMA construct, at day 5 of GFP-HUVEC seeding in the microchannels after removing the bioprinted *C. reinhardtii*-laden patterns by cellulase digestion. (B) Fluorescence micrographs showing live (green)/dead (red)-stained HepG2 cells in a GelMA construct and HUVECs in the microchannels at day 7 of HUVEC seeding.

(C) Viability of HepG2 cells in the GelMA matrices at day 3 and day 7 of HUVEC seeding in the microchannels. The control group had no HUVECs post-seeded into the microchannels. Results are presented as means  $\pm$  standard deviations.

(D) Viability of HUVECs at day 3 and day 7 of seeding in the microchannels. Results are presented as means  $\pm$  standard deviations.

(E) Fluorescence micrographs showing the immunostaining of CD31 expression (green) by the HUVECs at day 7 of HUVEC seeding in the microchannels. Nuclei were counterstained with DAPI (blue)

Finally, to generate the vascularized hepatic scaffolds, we seeded the hollow microchannels, formed after enzymatic removal of the C. reinhardtii-laden patterns, with human umbilical vein endothelial cells (HUVECs) at  $1.0-1.5 \times 10^7$  cells mL<sup>-1</sup> and continued incubation in DMEM/endothelial cell growth medium (1:1) for 7 days under standard cell-culture conditions. To facilitate visualization under fluorescence microscopy, we initially seeded green fluorescent protein (GFP)-HUVECs (green) in the microchannels while the HepG2 cells were stained with CM-Dil cell tracker (red) before encapsulation in the GelMA matrices (Figure 6A). The GFP-HUVECs were distributed evenly throughout the microchannels over the period of 7 days of culture. HUVECs without GFP were further seeded within the channels to evaluate the viability of HepG2 cells within the matrices and HUVECs within the microchannels by live/dead assay (Figure 6B). We assessed the viability of the HepG2 cells within the GelMA matrices after seeding HUVECs in the microchannels and compared it with that of the control samples in which the microchannels were kept empty (i.e., without HUVECs) after the removal of control bioprinted patterns (i.e., without C. reinhardtii). The viability of HepG2 cells was found to be higher (~91% at day 3 and  $\sim$ 92% at day 7) in the GelMA matrices wherein HepG2 cells were





co-cultured with C. reinhardtii-laden patterns during the early stages of culture and later seeded with HUVECs after removal of the C. reinhardtii-laden patterns. In contrast, the viability of HepG2 cells was approximately 70% at day 3 and 80% at day 7 in controls wherein bioprinted patterns without C. reinhardtii were embedded within HepG2/GelMA matrices and the microchannels that formed after removal of the bioprinted patterns were not seeded with HUVECs (Figure 6C). However, as largely expected, the viability of HepG2 cells within GelMA matrices was similar both before and after HUVEC seeding in the channels of the same scaffold. Similarly, the viability values of the HUVECs within the channels were approximately 83% at day 3 and 97% at day 7 (Figure 6D). To further confirm the formation of compact endothelial layer of HUVECs in the channels within hepatic scaffolds, we analyzed the expression of the intercellular endothelial junction marker, CD31, by HUVECs. For this, the hollow microchannels were seeded with HUVECs without GFP expression, followed by incubation in DMEM/endothelial cell growth medium (1:1) for 7 days. The immunofluorescence staining of HUVEC monolayers revealed strong CD31 expression, indicating the formation of tight junctions among the cells (Figure 6E). Thus, we demonstrated that the O<sub>2</sub> supplied by bioprinted C. reinhardtii within the tissue constructs boosted the viability of HepG2 cells during early days of co-culture, which supported the sustained viability and the metabolic activities of HepG2 cells within GelMA matrices that otherwise exhibited suppressed viability and functions even with the perfusion of vascular microchannels.

#### **DISCUSSION**

O<sub>2</sub> is required for most cell and tissue metabolic processes, and mitochondrial respiration accounts for the majority of O<sub>2</sub> consumption in humans, <sup>40</sup> where the aerobic metabolism of glucose generates adenosine-5'-triphosphate (ATP). Additionally, the citric acid cycle and  $\beta$ -oxidation of fatty acids are tightly coupled with the process of oxidative phosphorylation and production of ATP. These ATP molecules then provide the required energy for most physiological processes. Thus, O<sub>2</sub> bioavailability is vital to all cell functions and asserts its influence in regulating cell fate, morphogenesis, and organogenesis, among others. 41 On the other hand, green plants and algae synthesize ATP, reduce nicotinamide adenine dinucleotide phosphate (NADPH), and excrete O<sub>2</sub> by using light energy and water (H<sub>2</sub>O). <sup>42</sup> In the carbon-fixation cycle, glyceraldehyde-3-phosphate (G3P) is synthesized from carbon dioxide (CO<sub>2</sub>) and H<sub>2</sub>O by utilizing ATP and NADPH. Nutrients including carbohydrates are synthesized from G3P. CO<sub>2</sub>, produced by respiration, is reused as a core component in photosynthesis.<sup>28</sup> This "symbiotic recycling system" has been recently explored in in vitro tissue engineering to supply adequate O2 to mammalian cells and to reuse metabolites and waste products from mammalian cells. For example, C. sorokiniana was co-cultured with pancreatic islets encapsulated in alginate beads, which showed the generation of sufficient O2 by C. sorokiniana for respiration and function of islets under in vitro anoxic environments.<sup>26</sup>

 $O_2$  is a critical nutrient for maintaining the tissue microenvironment. <sup>43</sup> The sufficient supply of  $O_2$  and its diffusion into tissues are necessary for survival and physiological functions of tissues and organs. In adult human tissues,  $O_2$  concentration varies widely depending on the vasculature, metabolic requirements, and functions of each organ. For example, liver is one of the vital organs that plays major roles in balancing biochemical environments in the human body, including blood protein synthesis, glucose metabolism, fat metabolism, and detoxification of metabolites or other chemicals. The  $O_2$  consumption rate of rat hepatocytes was shown to be high, almost 10-fold higher than that of other cell types and 3-fold more within

## **Matter** Article



the first 24 h after the inoculation process, during the attachment, spreading, and reorganizing of the cells into confluent monolayers. <sup>44</sup> Similarly, it was shown that  $O_2$  is a critical factor for hepatocyte differentiation of human liver-derived cell lines, HepaRG and HepG2-C3A, and that increased levels of  $O_2$  lowers expression of HIF-1 $\alpha$  while increasing the expressions of albumin and hepatic transcription factor CEBP $\alpha$ , thus indicating the importance of pericellular  $O_2$  level for *in vitro* liver cell differentiation and functions. <sup>45</sup> Although various studies have been conducted to develop engineered 3D tissue constructs including the hepatic tissues, the lack of efficient  $O_2$  supply remains the primary limitation in tissue-engineered constructs. In general, 3D tissue constructs require functional and stable vascular networks to maintain the viability and biological functions of dense cell populations.

Here, we have presented a potent approach that integrates the use of 3D bioprinting of *C. reinhardtii* as a sustainable source of O<sub>2</sub> for liver-derived HepG2 cells embedded in volumetric hydrogel matrices, aiming at the fabrication of *in vitro* densified hepatic tissue constructs with maintained viability and functions. The unicellular green algae *C. reinhardtii* has long been used as a model microalgae for photosynthesis research, and 3D bioprinting is the process of additively depositing the bioink onto a surface to produce well-defined 3D structures to recapitulate organ- and tissue-level functionality, including the vasculature. <sup>46</sup> A bioink is essentially a hydrogel containing one or more types of living cells, biomaterials, and other growth supplements in various amounts, which mimics the extracellular matrix (ECM) of the desired tissue and supports the growth of the embedded cells. <sup>47</sup>

Considering that algal cell walls contain polysaccharides including cellulose, we selected a structurally relevant polymer, NaCMC, as the main component of the bioink for bioprinting of C. reinhardtii that supported its growth and proliferation. We used the cellulose-based sacrificial bioink formulation consisting of NaCMC, PVA, gelatin, and sodium alginate to facilitate the extrusion bioprinting of well-defined sacrificial patterns and the growth of C. reinhardtii. NaCMC is a water-soluble cellulose ether derivative of natural cellulose, in which sodium carboxymethyl groups (CH<sub>2</sub>COONa) are introduced into the cellulose molecules to promote water solubility. 48 The physical crosslinking of the NaCMC hydrogel occurs mainly through hydrogen bonding due to the presence of a large number of hydroxyl groups on the polymer chains. <sup>49,50</sup> Gelatin is a soluble polypeptide produced by partial hydrolysis of collagen, the major component of the natural ECM, and is a thermoreversible biopolymer with an upper critical solution temperature of approximately 30°C-35°C, i.e., it becomes liquid at above this temperature range, and at temperatures below roughly 25°C it forms a hydrogel. 51 Gelatin and gelatin-based hydrogels have been extensively used in developing in vitro tissue models because of their biocompatibility and biodegradability.<sup>52</sup> PVA is a water-soluble and biodegradable polyhydroxy polymer with high tensile strength. It is a synthetic polymer and has excellent adhesive properties.<sup>53</sup> The presence of hydroxyl groups attached to alternate carbons in PVA favors the formation of hydrogen bonding.<sup>54</sup> Alginate is a natural linear polysaccharide polymer that undergoes gelation by addition of divalent cations such as Ca<sup>2+</sup>, stabilizing the polymer network via physical crosslinking.<sup>55,56</sup> These polymers have been used widely in hydrogel preparations for applications in tissue engineering due to their biodegradability, biocompatibility, lack of toxicity, and cost-effectiveness.<sup>53</sup> The aim of our study is to use NaCMC-based bioink as the sacrificial matrix for bioprinting of C. reinhardtii and to apply the bioprinted C. reinhardtii-laden patterns as a living source of O<sub>2</sub> in the in vitro tissue constructs. The bioink formulations and their printability studies showed the optimal bioink formulation as 3% (v/v) NaCMC, 0.03% (v/v) PVA, 4% (v/v) gelatin, and 0.8% (v/v) alginate





at a pressure of 55 psi and feeding rate of 70 mm s $^{-1}$  when the 27-gauge extrusion nozzle was used (Figure 1).

The temperature and light conditions are the important factors for C. reinhardtii cultivation. Several studies have shown that temperature can significantly influence growth rate<sup>57</sup> and carbohydrate and lipid production,<sup>58</sup> as well as the induction of pigment formation.<sup>59</sup> While photoautotrophic growth occurs best between 25°C and 28°C for C. reinhardtii, 60 in these studies temperatures ranging from 10°C to 38°C were considered optimal based on the desired product. The viability assay of C. reinhardtii within bioprinted C. reinhardtii-laden patterns under continuous light exposure showed that the NaCMC-based hydrogel was compatible for the growth of C. reinhardtii and that these photosynthetic unicellular algae were bioprinting-friendly (Figure 2). Interestingly, the exposure of C. reinhardtii-laden patterns under a range of UV light did not have any adverse effect on the growth and chlorophyll content of the C. reinhardtii-laden patterns at both 25°C and 37°C (Figure S9). The effects of the attenuation of light illumination on the growth of C. reinhardtii and the subsequent O2 production were evaluated using tall cylindrical constructs approximately 6 cm high and 2 cm in diameter at both 25°C and 37°C. The attenuation of the growth and a consequent reduction in O<sub>2</sub> production by C. reinhardtii within the cylindrical constructs were observed with respect to the attenuation of illuminated light at both 25°C (Figures S10A and S10B) and 37°C (Figures \$10C and \$10D). It should be noted, however, that the overall size of the GelMA constructs was approximately 1-cm thick with 4 mm on the top and 4 mm at the bottom of the embedded, bioprinted C. reinhardtii. The GelMA layer (4 mm) on the top of the bioprinted C. reinhardtii pattern in each construct was transparent (Figures 3G and 3H) and was not so thick that it would significantly attenuate the illumination light and affect the growth of bioprinted C. reinhardtii within. Similar growth was observed at 37°C when the constructs were cultured in TAP medium. However, at 37°C they showed high cell viability for 4 days and gradually decreased over the period of 7 days in the presence or absence of GelMA matrices when grown in combined media (Figures 3E and S7).

In a related manner, when the C. reinhardtii-laden patterns were subjected to the 1-h/1-h light (2,800 lux)/dark cycles, the level of dissolved  $O_2$  in medium was found to increase gradually at both 25°C and 37°C over the culture period of 13 h and then decrease gradually until 20 h, followed by rapid reduction over 40 h (Figures S10E and S10F). Even though the dissolved  $O_2$  levels at 37°C and 25°C were comparable when the light was on, the  $O_2$  level was relatively low at 37°C when the light was off. In addition, the bioprinted C. reinhardtii-laden patterns showed high cell viability at 25°C over the period of 7 days both in the presence and absence of the surrounding GelMA matrices (Figures 3A and 3B). Similarly, these C. reinhardtii-laden patterns exhibited significant photosynthetic activities at both 25°C and 37°C over the period of 4 days under continuous light illumination (2,800 lux) in the presence as well as absence of the surrounding GelMA or HepG2/GelMA matrices (Figures 3C and 3F).

The excellent biocompatibility and the cellulase-mediated degradation<sup>38</sup> of NaCMC (Figure S3) have ensured the use of NaCMC-based hydrogel as the fugitive material for the bioprinting of photosynthetic algae, *C. reinhardtii*. The enzymatic digestion of the bioprinted NaCMC-based hydrogel patterns and *C. reinhardtii*-laden patterns in the presence or absence of the surrounding GelMA matrices suggested that the sacrificial NaCMC-based hydrogel, either with or without *C. reinhardtii*, could be effectively eliminated using cellulase (1 mg mL<sup>-1</sup> of cellulase in citrate buffer at pH 6) at both 25°C and 37°C, creating the interconnected microchannels within





the tissue constructs (Figures 3G and 3H). During the enzymatic digestion process, besides NaCMC, other major components of the bioink were also likely dissociated. The gelatin, PVA, and alginate components were added to improve the printability of the bioink and to stabilize the shapes of the bioprinted structures. The stable bioprinted patterns were formed mainly due to the intermolecular and/or intramolecular hydrogen bonding among the functional groups of the polymers present in the bioink<sup>35</sup> (Figure 1). The thermoreversible gelatin hydrogel formed was gradually dissolved out from the bioprinted pattern at temperatures higher than  $\sim 30^{\circ}$  C,  $^{61}$  leaving the spaces for rapid proliferation of C. reinhardtii within the bioprinted pattern. PVA is a biodegradable polymer that was present in very small amounts in the bioink, and alginate is a natural polymer that undergoes gelation by addition of divalent cations such as Ca<sup>2+</sup>. Therefore, when the NaCMC and/or C. reinhardtii component of a bioprinted structure was digested with cellulase, the entire pattern became easily dissolvable due to the damaged polymer network and significantly reduced hydrogen bonds, thus compromising overall stability. In addition, the treatment of C. reinhardtii-laden patterns embedded in HepG2/GelMA constructs with cellulase in citrate buffer at pH 6 did not have any negative influence on the HepG2 cells, which maintained higher levels of cell viability as well as reduced expression of HIF-1 $\alpha$  at day 7 compared with the control samples (Figure 4). Similarly, HepG2 cells within the constructs exhibited liver-specific functions, including F-actin organization, CYP3A4 and CYP1A2 protein expression, and albumin production as well as urea synthesis (Figure 5). Since prevascularization of in vitro tissue constructs is critical before implantation for proper O2 and nutrient diffusion and integration with host vasculature, 62 we finally seeded HUVECs in the hollow microchannels and proved that the cells were able to form a tight, confluent endothelium lining the inner surfaces of the microchannels within 7 days, thus generating the vascularized hepatic tissue-like constructs (Figure 6).

In summary, to develop vascularized tissue constructs with sufficient supply of  $O_2$  in vitro, our present study has presented 3D bioprinting of C. reinhardtii using NaCMC-based sacrificial bioink. The bioprinted C. reinhardtii-laden patterns served as a natural photosynthetic  $O_2$  generator within hepatic tissue constructs and supported the viability and functionality of the HepG2 cells within surrounding GelMA matrices. The enzymatic degradability of the bioprinted NaCMC-based patterns and C. reinhardtii further allowed the formation of hollow perfusable channels within the tissue constructs, which could then be endothelialized with a uniformly distributed layer of HUVECs.

Although the 3D bioprinting of C. reinhardtii and its applicability as a source of  $O_2$  for in vitro tissue constructs as well as formation of channels within the tissue constructs was achieved, more effort is likely needed to optimize the long-term co-culture systems. These include the development of optimized media that facilitate the co-culture of C. reinhardtii and human cells, as well as methods of illumination of light in the standard cell-culture incubators, among others, for sustained supply of  $O_2$  produced by the photosynthetic algae to the human cells and/or tissues in vitro. Further detailed studies on biosafety, toxicity, and immunocompatibility of algae are important for their application in vivo and possibly in clinical translation in the future. Besides, microalgae represent a rich source of several bioactive compounds such as protein, carbohydrates, polyunsaturated fatty acids, carotenoids, vitamins, and essential minerals, which when incorporated can enhance the nutritional value of food products, thus providing multiple health benefits.  $^{63-65}$  Such a 3D bioprinting technology can also be explored to develop various healthy innovative food products enriched with both animal and plant proteins or their subproducts.





#### **EXPERIMENTAL PROCEDURES**

#### **Resource Availability**

#### Lead Contact

Further information and requests for resources and reagents should be directed to and will be fulfilled by the Lead Contact, Yu Shrike Zhang (yszhang@research.bwh. harvard.edu).

#### Materials Availability

This study did not generate new unique reagents. Gelatin from porcine skin (type-A, 300 bloom), sodium alginate (low viscosity), methacrylic anhydride, CaCl<sub>2</sub>, NaCMC, cellulase from Aspergillus niger, 2-hydroxy-4'-(2-hydroxyethoxy)-2-methylpropiophenone (Irgacure 2959), Triton X-100, bovine serum albumin, and urea ELISA assay kit were purchased from Sigma-Aldrich (MO, USA). PVA ( $M_{\rm w}$  78,000 g mol<sup>-1</sup>) was obtained from Polysciences (PA, USA). Dulbecco's phosphate-buffered saline (DPBS), FBS, trypsin-ethylenediaminetetraacetic acid (trypsin-EDTA), P/S, DAPI, Live/Dead Viability/Cytotoxicity kit, PrestoBlue Cell Viability Reagent, Alexa Fluor 594-phalloidin, mouse CYP3A4/CYP3A5 monoclonal antibodies, Sytox-orange dead cell stain, and dialysis membrane ( $M_{w}$  cutoff 12-14 kDa) were obtained from Thermo Fisher Scientific (MA, USA). Endothelial cell growth medium was obtained from PromoCell (Germany). Mouse anti-HIF-1α antibody was obtained from Santa Cruz Biotechnology (CA, USA). Mouse anti-CD31 (P2B1) antibody, mouse anti-CYP1A2, Alexa Fluor 594-conjugated goat anti-mouse, and Alexa Fluor 488-conjugated goat anti-mouse secondary antibodies were purchased from Abcam (MA, USA). Human albumin ELISA kit was obtained from R&D Systems (MN, USA). Sylgard 184 silicone elastomer kit as was obtained from Dow Corning (MI, USA) for the fabrication of polydimethylsiloxane (PDMS) devices. Syringe filters (0.22 μm in pore size) were purchased from VWR International (MA, USA). The CellTiter 96 AQueous One Solution Cell Proliferation Assay kit was purchased from Promega (WI, USA). All other chemicals used in this study were obtained from Sigma-Aldrich unless otherwise mentioned.

#### Data and Code Availability

This study did not generate custom code, software, or algorithms. All data needed to evaluate the conclusions in the paper are present in the paper and/or Supplemental Information. Additional datasets that support the findings of this study are available from the corresponding authors upon reasonable request. All requests for raw and analyzed data and materials will be promptly reviewed by the Brigham and Women's Hospital to verify whether the request is subject to any intellectual property or confidentiality obligations. Any data and materials that can be shared will be released via a Material Transfer Agreement.

#### Cells

HepG2 cells and murine C2C12 myoblasts were obtained from American Type Culture Collection (VA, USA), whereas HUVECs with or without GFP labeling were purchased from Angio-Proteomie (MA, USA). HepG2 and C2C12 cells were cultured in DMEM supplemented with 10% FBS and 1% P/S while HUVECs were cultured in endothelial cell growth medium supplemented with the supplements. All cells were incubated at  $37^{\circ}\text{C}$  and 5% CO $_2$  in a humidified incubator until 80%–90% confluence. The respective culture medium was replaced every 3 days.

C. reinhardtii (+) was purchased from the Carolina Biological Supply Company (NC, USA) and grown on a standard TAP medium<sup>66</sup> in 500-mL Erlenmeyer flasks at 25°C under continuous light illumination of 2,800 lux using a relax LED bulb HD (General Electric Lighting, OH, USA). For all experiments, biological triplicates were





simultaneously grown to the mid-log phase (OD<sub>750</sub> 0.5–0.6) and cells were harvested by centrifuging at 1,000  $\times$  g for 5 min and discarding the supernatant.

#### **Synthesis of GelMA**

GelMA was synthesized as described previously.  $^6$  In brief, 10.0 g of type-A gelatin from porcine skin was dissolved in 100 mL of DPBS at  $60^{\circ}$ C, followed by addition of 8.0 mL of methacrylic anhydride dropwise with continuous stirring. The reaction was carried out at  $50^{\circ}$ C for 3 h and then quenched by a 5-fold dilution with warm DPBS ( $40^{\circ}$ C). The product was dialyzed with warm distilled water for 7 days using a dialysis membrane ( $M_{\rm w}$  cutoff 12–14 kDa), and finally lyophilized to obtain GelMA in the form of a white porous foam. The GelMA was stored at room temperature until further use.

#### **Preparation of Hydrogel Precursor Solutions and the Bioink**

The 10% (w/v) sodium alginate solution was prepared by dissolving sodium alginate powder in distilled water under continuous stirring overnight at 37°C. Similarly, 9% (w/v) NaCMC, 1.5% (w/v) of PVA, and 10% (w/v) gelatin solutions were prepared in distilled water, separately. All the prepolymer solutions were prepared in glass vials. The NaCMC solution was first mixed with PVA solution and then with gelatin and alginate solutions using a vortex mixer and incubated at 80°C for 1 h to obtain the homogeneous NaCMC-based hydrogel precursor solution (i.e., the bioink) containing 3% (v/v) NaCMC, 0.03% (v/v) PVA, 4% (v/v) gelatin, and 0.8% (v/v) alginate. This homogeneous NaCMC-based hydrogel solution was sterilized by filtration through a sterile 0.22-μm filter. The 0.3-M CaCl<sub>2</sub> solution was prepared by dissolving CaCl<sub>2</sub> powder in deionized water, autoclaved at 121°C for 15 min, and stored at 4°C until use.

The 5% (w/v) GelMA hydrogel precursor solution containing 0.3% (w/v) Irgacure 2959 was prepared by dissolving GelMA and Irgacure 2959 powder in DPBS at  $50^{\circ}$ C and sterilized by filtration through a sterile 0.22- $\mu$ m filter.

#### **Viscosity Measurements**

The viscosity profiles of the NaCMC-based bioink and its individual components at optimized concentration (3% (v/v) NaCMC, 0.03% (v/v) PVA, 4% (v/v) gelatin, and 0.8% (v/v) alginate) were measured with a hybrid rheometer (HR-3, Waters, VA, USA). All the individual components and the bioink, at the optimized concentrations, were maintained at 25°C until their viscosity values were measured under a shear ramp mode running from 0.01 to 1,000 s<sup>-1</sup> with a 1,000- $\mu$ m gap size at 25°C.

#### 3D Bioprinting of C. reinhardtii-Containing Bioinks

Various bioink compositions containing different amount of NaCMC (3%–10% v/v), PVA (0.01%–0.1% v/v), gelatin (2%–10% w/v), and alginate (0.5%–1% w/v) were tested for the printability of the predesigned geometry at different pressures (35–60 psi) and at different feeding rates (60–100 mm s<sup>-1</sup>). The homogeneous mixture of NaCMC, PVA, gelatin, and alginate solutions that gave the best results at a given pressure and feeding rate was used as the matrix for bioprinting of *C. reinhardtii*. Immediately prior to bioprinting, a suspension of *C. reinhardtii* was pelleted and different densities of *C. reinhardtii* (1.0–10 × 10<sup>6</sup> cells mL<sup>-1</sup>) were resuspended in the bioink. The bioink with or without *C. reinhardtii* was loaded into a 10-mL syringe (BD Biosciences, MA, USA) fitted with a 27-gauge blunt needle, and extrusion bioprinting was performed using a bioprinter (Allevi 2, PA, USA) with digitally controlled pneumatic pressures, followed by crosslinking with the 0.3-M CaCl<sub>2</sub> solution. Pressure to drive the syringe pistons was supplied by an in-house nitrogen line and





maintained at approximately 55 psi by pressure regulators and gauges while the bioink feeding rate was kept constant at 70 mm s $^{-1}$ . The bioink without *C. reinhardtii* was used for bioprinting of scaffolds to be used as the control groups.

#### Characterizations of 3D-Bioprinted C. reinhardtii Patterns

The 3D-bioprinted *C. reinhardtii* patterns were incubated in the TAP medium at 25°C under illumination by LED light bulbs (light intensity 2,800 lux). Viability and growth of the algae were evaluated by measuring the OD at 750 nm at different time points and different temperatures (25°C and 37°C). In addition, live/dead assay was performed by using the Sytox-orange fluorescent probe, with excitation and emission peaks of 547 nm and 570 nm, respectively, according to the manufacturer's instructions. In brief, the bioprinted *C. reinhardtii* patterns were incubated in the TAP medium containing 5  $\mu$ M Sytox-orange fluorescent probe for 5 min at 25°C in darkness. The Sytox-orange dye could penetrate damaged cell membranes and therefore stain dead cells in orange, whereas viable cells would exhibit the red autofluorescence of chlorophyll. The samples were analyzed using a Zeiss Axio Observer inverted fluorescence microscope (Zeiss, NY, USA).

#### **Measurement of Chlorophyll**

Chlorophyll contents in the bioprinted *C. reinhardtii* patterns were determined at day 7 using an ethanol extraction method. <sup>67,68</sup> One milliliter of 95% ethanol was added to each of the bioprinted *C. reinhardtii* patterns and vortexed to extract green pigments at room temperature. It was then centrifuged at 3,000  $\times$  g for 5 min and absorption was measured at 665 nm with a microplate reader (Tecan, Austria).

#### Measurements of O<sub>2</sub> Release from the 3D-Bioprinted C. reinhardtii Patterns

Dissolved  $O_2$  present in the TAP medium was removed by flushing with a nitrogen gas for 20 min, followed by incubation with the bioprinted C. reinhardtii patterns at 25°C and/or 37°C. Thus, photoautotrophic  $O_2$  release by C. reinhardtii was measured by changes of  $O_2$  concentrations in the medium using a dissolved  $O_2$  sensor kit (Atlas Scientific, NY, USA) according to manufacturer's instructions. Similarly, the  $O_2$  levels released by the bioprinted C. reinhardtii patterns embedded within GelMA hydrogel constructs were also measured.

#### **Fabrication of Vascularized 3D Hepatic Tissue-like Constructs**

The 3D-bioprinted NaCMC-based *C. reinhardtii* patterns were gently washed with DPBS and embedded in 5% GelMA hydrogels containing HepG2 cells to generate the hepatic tissue constructs. The bioprinted *C. reinhardtii*-laden constructs were embedded in GelMA hydrogel precursor solution with or without HepG2 cells and crosslinked with UV light (6.9 mW cm<sup>-2</sup>) for 40 s. The overall size of the tissue constructs was approximately 1-cm thick with 4 mm of GelMA on the top and 4 mm at the bottom of the embedded, bioprinted *C. reinhardtii*. The constructs were incubated in TAP medium or DMEM/TAP medium (1:1) for 3 days at 25°C or 37°C under 5% CO<sub>2</sub> in a humidified incubator and at day 4, the samples were treated with 1 mg mL<sup>-1</sup> of cellulase in citrate buffer (pH 6) for 2–24 h. The enzymatic removal of the sacrificial *C. reinhardtii*-laden constructs was confirmed by observation under an optical and fluorescent microscope. The 3D-bioprinted patterns without *C. reinhardtii* were used as the control.

#### **Cell Viability and Proliferation Assays**

The viability of HepG2 cells in the constructs was evaluated by live/dead assay using the Live/Dead Viability/Cytotoxicity kit (for mammalian cells) according to the manufacturer's instructions. For the cell viability assay, the constructs were washed three times with DPBS and incubated with 500  $\mu$ L well<sup>-1</sup> of the combined live/dead assay





reagents (2  $\mu$ M calcein AM and 4  $\mu$ M ethidium homodimer I) for 20 min at 37°C in the dark. The cells were then washed with DPBS and observed under the fluorescence microscope. The MTS assay was performed using the CellTiter 96 AQueous One Solution Cell Proliferation Assay kit. The media were removed and the constructs incubated with MTS assay solution for 2 h at 37°C in darkness. The absorbance was measured at 492 nm with a microplate reader, and the results were expressed as percentages of the control. All the experiments were conducted in triplicates and were repeated three times.

#### Measurements of Secreted Albumin and Urea

The concentrations of albumin secreted by the cells in the constructs were measured using ELISA according to the manufacturer's protocol. The HepG2 constructs with embedded bioprinted patterns, with or without C. reinhardtii, were cultured at  $37^{\circ}C$  and 5%  $CO_2$  in a humidified incubator for 3 days and then treated with 1 mg mL $^{-1}$  cellulase in citrate buffer for 2 h to digest the bioink and C. reinhardtii. The samples were further incubated  $37^{\circ}C$  until day 7. The culture supernatants were collected at days 3 and 7 and stored at  $-80^{\circ}C$  until analysis.

For albumin assay, all the reagents were brought to the room temperature before starting the assay. A 50- $\mu L$  amount of standard or sample was added to each well of albumin ELISA plate and 50  $\mu L$  of the antibody cocktail was added to each well and incubated for 1 h at room temperature. Each well was then washed three times with Wash Buffer PT. Next, 100  $\mu L$  of TMB development solution was added to each well and incubated for 10 min in darkness, followed by three washes. Finally, 100  $\mu L$  of the stop solution was added to each well and incubated for 1 min, and the OD was recorded at 450 nm with the microplate reader.

Similarly, measurement of urea contents was performed using the Urea Assay Kit according to the manufacturer's instructions. In brief, 0, 1, 2, 3, 4, and 5 nmol well $^{-1}$  of urea standards were prepared by diluting 100 nmol  $mL^{-1}$  of urea standard solution with urea assay buffer, and 50  $\mu L$  of each of the standard urea and 50  $\mu L$  of each sample were placed in separate wells of a flat-bottom 96-well plate. Next, 50  $\mu L$  of the freshly prepared reaction mix was added to each well and mixed quickly by gently rocking the plate. The reaction was then incubated at 37°C for 1 h in darkness and absorbance was measured at 570 nm on the microplate reader. The samples were run in triplicates unless otherwise stated.

#### F-Actin Staining of the Cells

The cells in the constructs were washed with DPBS, fixed with 4% (v/v) paraformaldehyde for 15 min, and permeabilized with 0.1% (v/v) Triton X-100 in DPBS for 1 h. The samples were then blocked with 5% (w/v) goat serum in DPBS for 1 h, followed by F-actin staining by incubating the samples with Alexa Fluor 594-phalloidin (1:200 dilution in blocking buffer) overnight at 4°C. After washing with DPBS, the nuclei were counterstained with DAPI (1:1,000) for 5 min at room temperature. Finally, the cells in the constructs were observed under the fluorescence microscope.

#### **Immunocytochemical Analyses**

For evaluation of the hypoxia conditions and demonstration of the functions of HepG2 cells within the tissue constructs in the presence or the absence of *C. reinhardtii*, the cells were immunostained for HIF-1 $\alpha$ , CYP3A4, and CYP1A2. At day 7, the cells were washed with DPBS and fixed with 4% (w/v) paraformaldehyde for 30 min at room temperature, followed by incubation with the permeabilization





buffer (0.1% [v/v] Triton X-100 in DPBS) for 1 h at room temperature. The cells were then blocked with 5% (w/v) goat serum in DPBS for 2 h at room temperature and incubated with respective primary antibodies (1:200 dilution) overnight at 4°C. The samples were washed with DPBS and incubated with the corresponding secondary antibody at 1:200 dilution (Alexa Fluor 594-conjugated goat anti-mouse antibody or Alexa Fluor 488-conjugated goat anti-mouse antibody) overnight at 4°C. Finally, the nuclei were counterstained with DAPI after washing with DPBS and examined under the fluorescence microscope. Similarly, HUVECs in the channels were immunostained with primary mouse anti-CD31 antibody and secondary Alexa Fluor 488-goat anti-mouse antibody.

#### **Statistical Analysis**

All experiments were performed in triplicates and the results presented as mean  $\pm$ standard deviation. Statistical analyses were performed by paired t test using Graph-Pad Prism (CA, USA) and p  $\leq$  0.05 was considered as statistically significant (\*p  $\leq$ 0.05, \*\*p  $\leq 0.01$ , \*\*\*p  $\leq 0.001$  in figures).

#### SUPPLEMENTAL INFORMATION

Supplemental Information can be found online at https://doi.org/10.1016/j.matt. 2020.10.022.

#### **ACKNOWLEDGMENTS**

This work was supported by funding from the National Institutes of Health (K99CA201603, R00CA201603, R21EB025270, R21EB026175, R01EB028143, R01GM134036), National Science Foundation (1936105), the National Science Foundation (1936105), and the Brigham Research Institute.

#### **AUTHOR CONTRIBUTIONS**

S.M. designed and performed the experiments, collected and analyzed the data, and prepared the manuscript; J.A., C.C., A.G.R., D.H, C.D., E.C., M.D.R., D.B., M.L.S, W.L., F.C., and G.Y. performed the experiments and revised the manuscript; Y.S.Z. conceptualized, designed, and supported the study, and prepared the manuscript.

#### **DECLARATION OF INTERESTS**

The authors declare no competing interest.

Received: March 2, 2020 Revised: September 27, 2020 Accepted: October 16, 2020 Published: November 18, 2020

#### **REFERENCES**

- 1. Matesanz, R., Mahíllo, B., Álvarez, M., and Carmona, M. (2009). Global observatory and database on donation and transplantation: world overview on transplantation activities. Transplant. Proc. 41, 2297-2301.
- 2. Giwa, S., Lewis, J.K., Alvarez, L., Langer, R., Roth, A.E., Church, G.M., Markmann, J.F., Sachs, D.H., Chandraker, A., and Wertheim, J.A. (2017). The promise of organ and tissue preservation to transform medicine. Nat. Biotechnol. 35, 530.
- 3. Atala, A., Kasper, F.K., and Mikos, A.G. (2012). Engineering complex tissues. Sci. Transl. Med. 4, 160rv12.
- 4. Zhang, Y.S., Yue, K., Aleman, J., Mollazadeh-Moghaddam, K., Bakht, S.M., Yang, J., Jia, W., Dell'Erba, V., Assawes, P., and Shin, S.R. (2017). 3D bioprinting for tissue and organ fabrication. Ann. Biomed. Eng. 45, 148-163.
- 5. Ying, G.L., Jiang, N., Maharjan, S., Yin, Y.X., Chai, R.R., Cao, X., Yang, J.Z., Miri, A.K., Hassan, S., and Zhang, Y.S. (2018). Aqueous
- two-phase emulsion bioink-enabled 3D bioprinting of porous hydrogels. Adv. Mater. 30, 1805460.
- 6. Pi, Q., Maharjan, S., Yan, X., Liu, X., Singh, B., van Genderen, A.M., Robledo-Padilla, F Parra-Saldivar, R., Hu, N., and Jia, W. (2018). Digitally tunable microfluidic bioprinting of multilayered cannular tissues. Adv. Mater. 30, 1706913.
- 7. Fernandez, C., Yen, R., Perez, S., Bedell, H., Povsic, T., Reichert, W., and Truskey, G. (2016).

## **Matter**

#### Article



- Human vascular microphysiological system for in vitro drug screening. Sci. Rep. 6, 21579.
- Ma, X., Liu, J., Zhu, W., Tang, M., Lawrence, N., Yu, C., Gou, M., and Chen, S. (2018). 3D bioprinting of functional tissue models for personalized drug screening and in vitro disease modeling. Adv. Drug Deliv. Rev. 132, 235–251.
- Mazzocchi, A., Soker, S., and Skardal, A. (2019).
  D bioprinting for high-throughput screening: drug screening, disease modeling, and precision medicine applications. Appl. Phys. Rev. 6, 011302.
- Rouwkema, J., Koopman, B.F., Blitterswijk, C.A.V., Dhert, W.J., and Malda, J. (2009). Supply of nutrients to cells in engineered tissues. Biotechnol. Genet. Eng. 26, 163–178.
- Sarker, M., Chen, X., and Schreyer, D. (2015). Experimental approaches to vascularisation within tissue engineering constructs.
   J. Biomater. Sci. Polym. Ed. 26, 683–734.
- Lewis, M.C., MacArthur, B.D., Malda, J., Pettet, G., and Please, C.P. (2005). Heterogeneous proliferation within engineered cartilaginous tissue: the role of oxygen tension. Biotechnol. Bioeng. 91, 607–615.
- Kolesky, D.B., Homan, K.A., Skylar-Scott, M.A., and Lewis, J.A. (2016). Three-dimensional bioprinting of thick vascularized tissues. Proc. Natl. Acad. Sci. U S A 113, 3179–3184.
- 14. McQuilling, J.P., Sittadjody, S., Pendergraft, S., Farney, A.C., and Opara, E.C. (2017). Applications of particulate oxygen-generating substances (POGS) in the bioartificial pancreas. Biomater. Sci. 5, 2437–2447.
- Harrison, B.S., Eberli, D., Lee, S.J., Atala, A., and Yoo, J.J. (2007). Oxygen producing biomaterials for tissue regeneration. Biomaterials 28, 4628–4634.
- Pedraza, E., Coronel, M.M., Fraker, C.A., Ricordi, C., and Stabler, C.L. (2012). Preventing hypoxia-induced cell death in beta cells and islets via hydrolytically activated, oxygengenerating biomaterials. Proc. Natl. Acad. Sci. U S A 109, 4245–4250.
- Abdi, S.I.H., Ng, S.M., and Lim, J.O. (2011). An enzyme-modulated oxygen-producing microsystem for regenerative therapeutics. Int. J. Pharm. 409, 203–205.
- 18. Oh, S.H., Ward, C.L., Atala, A., Yoo, J.J., and Harrison, B.S. (2009). Oxygen generating scaffolds for enhancing engineered tissue survival. Biomaterials 30, 757–762.
- Li, Z., Guo, X., and Guan, J. (2012). An oxygen release system to augment cardiac progenitor cell survival and differentiation under hypoxic condition. Biomaterials 33, 5914–5923.
- Gholipourmalekabadi, M., Zhao, S., Harrison, B.S., Mozafari, M., and Seifalian, A.M. (2016). Oxygen-generating biomaterials: a new, viable paradigm for tissue engineering? Trends Biotechnol. 34, 1010–1021.
- Lee, V.K., Lanzi, A.M., Ngo, H., Yoo, S.-S., Vincent, P.A., and Dai, G. (2014). Generation of multi-scale vascular network system within 3D hydrogel using 3D bio-printing technology. Cell. Mol. Bioeng. 7, 460–472.

- Zhang, Y.S., Davoudi, F., Walch, P., Manbachi, A., Luo, X., Dell'Erba, V., Miri, A.K., Albadawi, H., Arneri, A., and Li, X. (2016). Bioprinted thrombosis-on-a-chip. Lab Chip. 16, 4097– 4105.
- Cheng, F., Cao, X., Li, H., Liu, T., Xie, X., Huang, D., Maharjan, S., Bei, H.P., Gómez, A., and Li, J. (2019). Generation of cost-effective paperbased tissue models through matrix-assisted sacrificial 3D printing. Nano Lett. 6, 3603–3611.
- Hegen, A., Blois, A., Tiron, C.E., Hellesøy, M., Micklem, D.R., Nör, J.E., Akslen, L.A., and Lorens, J.B. (2011). Efficient in vivo vascularization of tissue-engineering scaffolds. J. Tissue Eng. Regen. Med. 5, e52–e62.
- Wang, Z., He, Y., Yu, X., Fu, W., Wang, W., and Huang, H. (2012). Rapid vascularization of tissue-engineered vascular grafts in vivo by endothelial cells in co-culture with smooth muscle cells. J. Mater. Sci. Mater. Med. 23, 1109–1117.
- Bloch, K., Papismedov, E., Yavriyants, K., Vorobeychik, M., Beer, S., and Vardi, P. (2006). Photosynthetic oxygen generator for bioartificial pancreas. Tissue Eng. 12, 337–344.
- Hopfner, U., Schenck, T.-L., Chávez, M.-N., Machens, H.-G., Bohne, A.-V., Nickelsen, J., Giunta, R.-E., and Egaña, J.-T. (2014).
   Development of photosynthetic biomaterials for in vitro tissue engineering. Acta Biomater. 10, 2712–2717.
- Haraguchi, Y., Kagawa, Y., Sakaguchi, K., Matsuura, K., Shimizu, T., and Okano, T. (2017). Thicker three-dimensional tissue from a "symbiotic recycling system" combining mammalian cells and algae. Sci. Rep. 7, 41594.
- Lode, A., Krujatz, F., Brüggemeier, S., Quade, M., Schütz, K., Knaack, S., Weber, J., Bley, T., and Gelinsky, M. (2015). Green bioprinting: fabrication of photosynthetic algae-laden hydrogel scaffolds for biotechnological and medical applications. Eng. Life Sci. 15, 177–183.
- Hon, D.N.-S. (1996). Cellulose and its derivatives: structures, reactions, and medical uses. In Polysaccharides in Medicinal Applications, S. Dumitriu, ed. (Taylor & Francis Group), pp. 87–106.
- 31. Dutta, S.D., Patel, D.K., and Lim, K.-T. (2019). Functional cellulose-based hydrogels as extracellular matrices for tissue engineering. J. Biol. Eng. 13, 55.
- **32.** Sannino, A., Demitri, C., and Madaghiele, M. (2009). Biodegradable cellulose-based hydrogels: design and applications. Materials *2*, 353–373.
- Lopez, C.G., Colby, R.H., and Cabral, J.o.T. (2018). Electrostatic and hydrophobic interactions in NaCMC aqueous solutions: effect of degree of substitution. Macromolecules 51, 3165–3175.
- Ribeiro, A., Blokzijl, M.M., Levato, R., Visser, C.W., Castilho, M., Hennink, W.E., Vermonden, T., and Malda, J. (2017). Assessing bioink shape fidelity to aid material development in 3D bioprinting. Biofabrication 10, 014102.
- 35. Hu, W., Wang, Z., Xiao, Y., Zhang, S., and Wang, J. (2019). Advances in crosslinking

- strategies of biomedical hydrogels. Biomater. Sci. 7, 843–855.
- Eo, M.Y., Fan, H., Cho, Y.J., Kim, S.M., and Lee, S.K. (2016). Cellulose membrane as a biomaterial: from hydrolysis to depolymerization with electron beam. Biomater. Res. 20, 16.
- Zhivkov, A.M. (2013). Electric properties of carboxymethyl cellulose. In Cellulose: Fundamental Aspects, T. van de Ven and L Godbout, eds. (IntechOpen), pp. 197–226.
- Fei, B., Wach, R.A., Mitomo, H., Yoshii, F., and Kume, T. (2000). Hydrogel of biodegradable cellulose derivatives. I. Radiation-induced crosslinking of CMC. J. Appl. Polym. 78, 278–283.
- Zanger, U.M., Schwab, M., and therapeutics. (2013). Cytochrome P450 enzymes in drug metabolism: regulation of gene expression, enzyme activities, and impact of genetic variation. Pharmacol. Ther. 138, 103–141.
- Boveris, A., Costa, L.E., Cadenas, E., and Poderoso, J.J. (1999). Regulation of mitochondrial respiration by adenosine diphosphate, oxygen, and nitric oxide. Methods Enzymol. 301, 188–198.
- Fathollahipour, S., Patil, P.S., and Leipzig, N.D. (2018). Oxygen regulation in development: lessons from embryogenesis towards tissue engineering. Cells Tissues Organs 205, 350–371.
- 42. Alberts, B., Johnson, A., Lewis, J., Raff, M., Roberts, K., and Walter, P. (2002). Energy conversion: mitochondria and chloroplasts. Molecular Biology of the Cell, Fourth Edition (Garland Science), pp. 815–878.
- Xiao, W., Shinohara, M., Komori, K., Sakai, Y., Matsui, H., and Osada, T. (2014). The importance of physiological oxygen concentrations in the sandwich cultures of rat hepatocytes on gas-permeable membranes. Biotechnol. Prog. 30, 1401–1410.
- Matsui, H., Osada, T., Moroshita, Y., Sekijima, M., Fujii, T., Takeuchi, S., and Sakai, Y. (2010). Rapid and enhanced repolarization in sandwich-cultured hepatocytes on an oxygenpermeable membrane. Biochem. Eng. J. 52, 255–262.
- 45. van Wenum, M., Adam, A.A., van der Mark, V.A., Chang, J.-C., Wildenberg, M.E., Hendriks, E.J., Jongejan, A., Moerland, P.D., van Gulik, T.M., and Elferink, R.P.O. (2018). Oxygen drives hepatocyte differentiation and phenotype stability in liver cell lines. Cell Commun. Signal. 12, 575–588.
- 46. Datta, P., Ayan, B., and Ozbolat, I.T. (2017). Bioprinting for vascular and vascularized tissue biofabrication. Acta Biomater. 51, 1–20.
- 47. Chimene, D., Lennox, K.K., Kaunas, R.R., and Gaharwar, A.K. (2016). Advanced bioinks for 3D printing: a materials science perspective. Ann. Biomed. Eng. 44, 2090–2102.
- Wüstenberg, T. (2014). Sodium carboxymethylcellulose. In Cellulose and Cellulose Derivatives in the Food Industry, T. Wüstenberg, ed. (Wiley-VCH), pp. 387–478.
- 49. Edgar, K.J., Buchanan, C.M., Debenham, J.S., Rundquist, P.A., Seiler, B.D., Shelton, M.C., and





- Tindall, D. (2001). Advances in cellulose ester performance and application. Prog. Polym. Sci. 26, 1605–1688.
- Shen, X., Shamshina, J.L., Berton, P., Gurau, G., and Rogers, R.D. (2016). Hydrogels based on cellulose and chitin: fabrication, properties, and applications. Green. Chem. 18, 53–75.
- Joly-Duhamel, C., Hellio, D., and Djabourov, M. (2002). All gelatin networks: 1. Biodiversity and physical chemistry. Langmuir 18, 7208– 7217.
- 52. Pelling, A.E., Hickey, R.J., and Biotechnology. (2019). Cellulose biomaterials for tissue engineering. Front. Bioeng. Biotechnol. 7, 45.
- Peng, Z., and Shen, Y. (2011). Study on biological safety of polyvinyl alcohol/collagen hydrogel as tissue substitute (I). Polym. Plast. Technol. Eng. 50, 245–250.
- 54. Briscoe, B., Luckham, P., and Zhu, S. (2000). The effects of hydrogen bonding upon the viscosity of aqueous poly (vinyl alcohol) solutions. Polym. J. 41, 3851–3860.
- Lee, K.Y., and Mooney, D.J. (2012). Alginate: properties and biomedical applications. Prog. Polym. Sci. 37, 106–126.

- Augst, A.D., Kong, H.J., and Mooney, D.J. (2006). Alginate hydrogels as biomaterials. Macromol. Biosci. 6, 623–633.
- Xin, L., Hong-Ying, H., and Yu-Ping, Z. (2011). Growth and lipid accumulation properties of a freshwater microalga *Scenedesmus* sp. under different cultivation temperature. Bioresour. Technol. 102, 3098–3102.
- Subhash, G.V., Rohit, M., Devi, M.P., Swamy, Y., and Mohan, S.V. (2014). Temperature induced stress influence on biodiesel productivity during mixotrophic microalgae cultivation with wastewater. Bioresour. Technol. 169, 789–793.
- Markou, G., and Nerantzis, E. (2013). Microalgae for high-value compounds and biofuels production: a review with focus on cultivation under stress conditions. Biotechnol. Adv. 31, 1532–1542.
- Adams, G.M.W., Huang, B., and Luck, D.J. (1982). Temperature-sensitive, assemblydefective flagella mutants of *Chlamydomonas* reinhardtii. Genetics 100, 579–586.
- Yin, J., Yan, M., Wang, Y., Fu, J., and Suo, H. (2018). 3D bioprinting of low-concentration cell-laden gelatin methacrylate (GelMA) bioinks with a two-step cross-linking strategy. ACS Appl. Mater. Inter. 10, 6849–6857.

- Lovett, M., Lee, K., Edwards, A., and Kaplan, D.L. (2009). Vascularization strategies for tissue engineering. Tissue Eng. B Rev. 15, 353–370.
- Chacón-Lee, T.L., and González-Mariño, G.E. (2010). Microalgae for "healthy" foods possibilities and challenges. Compr. Rev. Food Sci. Food Saf. 9, 655–675.
- Matos, Ã.N.P. (2017). The impact of microalgae in food science and technology. J. Am. Oil Chem. Soc. 94, 1333–1350.
- Camacho, F., Macedo, A., and Malcata, F. (2019). Potential industrial applications and commercialization of microalgae in the functional food and feed industries: a short review. Mar. Drugs 17, 312.
- Harris, E.H., Stern, D.B., and Witman, G.B. (2009). The Chlamydomonas Sourcebook, Vol. 1 (Academic Press).
- Berberoglu, H., Pilon, L., and Melis, A. (2008). Radiation characteristics of Chlamydomonas reinhardtii CC125 and its truncated chlorophyll antenna transformants tla1, tlaX and tla1-CW+. Int. J. Hydrogen Energy 33, 6467–6483.
- Wintermans, J.F.G.M., and De Mots, A. (1965). Spectrophotometric characteristics of chlorophylls a and b and their phenophytins in ethanol. Biochim. Biophys. Acta 109, 448–453.